universität wien

MASTERARBEIT / MASTER'S THESIS

Titel der Masterarbeit / Title of the Master's Thesis

„The importance of vinyl ether and non-vinyl ether phospholipids on mouse behavior "

verfasst von / submitted by

Erik Harrucksteiner, BSc

angestrebter akademischer Grad / in partial fulfilment of the requirements for the degree of

Magister pharmaciae (Mag.pharm.)

Wien, 2023 / Vienna 2023

Studienkennzahl lt. Studienblatt / degree programme code as it appears on the student record sheet:	UA 066 605
Studienrichtung lt. Studienblatt / degree programme as it appears on the student record sheet:	Masterstudium Pharmazie
Betreut von / Supervisor:	Univ.Prof. Dr. Johannes Berger

ACKNOWLEDGMENTS

First, I want to thank my thesis advisor Johannes Berger not only for his warm welcome quickly making me feel part of his team but also for the opportunity to work on this exciting project as well as allowing me insight and hands on experience into other aspects of the project. I'm thankful for his contagious enthusiasm also making me passionate about the project and his patience, motivation and support throughout the entire time I was part of the project.

My genuine thanks also go to Sylvia Badurek and Klaus Kraitsy, who supervised me in the Vienna BioCenter and always helped me whenever I had a question or when I was stuck in the changing room.

I would also like to sincerely thank Fabian Dorninger for his helpful guidance, his detailed insights, and his quick and reliable response whenever something was unclear to me.

Furthermore, I would like to thank all the members of the Berger lab for the encouragement, the helpful support and the fun coffee breaks keeping me motivated.

Lastly, I want to thank my family and friends for always encouraging and supporting me throughout my years of study.

TABLE OF CONTENTS

LIST OF FIGURES

ABSTRACT

The inherited metabolic disease rhizomelic chondrodysplasia punctata (RCDP) is caused by mutations in peroxisomal enzymes involved in the biosynthesis of ether phospholipids. These form a subgroup of phospholipids and perform a variety of different functions in mammals. The most abundant subgroup of ether phospholipids are vinyl ether phospholipids that are enriched in the brain and heart and play an important role in brain development, cognitive processes and signal transduction. Most importantly, they are structure-giving components of cellular membranes and facilitate membrane fusion and fission processes. A lack of vinyl ether phospholipids in mice resulted in complex behavioral abnormalities mimicking aspects of human psychiatric disorders, particularly autism and attention-deficit hyperactivity disorder.

In order to elucidate the importance of vinyl ether and non-vinyl ether phospholipids on mouse behavior a three-chamber social interaction approach, metabolic cage trial (TSE PhenoMaster) and fear conditioning were conducted using *Gnpat* KO (lacking all ether phospholipids), *Peds1* KO (lacking only vinyl-ether phospholipids) and wildtype animals as controls.

Our study showed no significant differences within each genotype and between the genotypes in social interaction, even though trends were visible. Locomotor activity, energy expenditure, oxygen consumption and carbon dioxide production were significantly increased in both *Gnpat* KO and *Peds1* KO compared to WT animals. *Gnpat* KO and *Peds1* KO mice displayed significantly reduced freezing response in contextual and cued fear conditioning, suggesting impaired associative learning and memory.

In conclusion, our findings highlight the importance of vinyl ether phospholipids and non-vinyl ether phospholipids on mouse behavior as well as for metabolism.

KURZFASSUNG

Die erbliche Stoffwechselkrankheit rhizomelische Chondrodysplasie punctata (RCDP) wird durch Mutationen in peroxisomalen Enzymen verursacht, die an der Biosynthese von Etherphospholipiden beteiligt sind. Diese bilden eine Untergruppe der Phospholipide und erfüllen bei Säugetieren eine Vielzahl unterschiedlicher Funktionen. Die am häufigsten vorkommende Untergruppe der Etherphospholipide sind die Vinyletherphospholipide, die im Gehirn und im Herzen angereichert sind und eine wichtige Rolle bei der Gehirnentwicklung, kognitiven Prozessen und der Signalübertragung spielen. Vor allem aber sind sie strukturgebende Bestandteile von Zellmembranen und erleichtern Membranfusions- und Abschnürungsprozesse. Ein Mangel an Vinyletherphospholipiden bei Mäusen führte zu komplexen Verhaltensanomalien, die Aspekte menschlicher psychiatrischer Störungen, insbesondere Autismus und Aufmerksamkeitsdefizit-Hyperaktivitätsstörung, nachahmen. Um die Bedeutung von Vinylether- und Nicht-Vinylether-Phospholipiden für das Verhalten von Mäusen zu klären, wurden ein Drei-Kammer-Ansatz zur sozialen Interaktion, ein metabolischer Käfigversuch (TSE PhenoMaster) und Angstkonditionierung mit *Gnpat* KO (dem alle Ether-Phospholipide fehlen), *Peds1* KO (dem nur Vinylether-Phospholipide fehlen) und Wildtyp-Tieren als Kontrollen durchgeführt.

Unsere Studie zeigte keine signifikanten Unterschiede innerhalb der einzelnen Genotypen und zwischen den Genotypen betreffend sozialer Interaktion, obwohl Tendenzen erkennbar waren. Lokomotorische Aktivität, Energieverbrauch, Sauerstoffverbrauch und Kohlendioxidproduktion waren sowohl bei *Gnpat* KO als auch bei *Peds1* KO im Vergleich zu WT-Tieren signifikant erhöht. *Gnpat* KO- und *Peds1* KO-Mäuse zeigten bei der kontextuellen und kognitiven Angstkonditionierung ein signifikant reduziertes Erstarren, was auf eine Beeinträchtigung des assoziativen Lernens und Gedächtnisses hindeutet.

Zusammengefasst unterstreichen unsere Ergebnisse die Bedeutung von Vinyletherphospholipiden und Nicht-Vinyletherphospholipiden für das Verhalten von Mäusen sowie für den Stoffwechsel.

ABBREVIATIONS

1-O-alkyl-G3P – 1-O-alkyl-glycerol-3-phosphate

AA – arachidonic acid

ADHAPR – acyl/alkyl-dihydroxyacetone-3-phosphate reductase

ADHAPS – alkyl-dihydroxyacetone phosphate synthase

AGPS – alkylglycerone phosphate synthase

CNS – central nervous system

CS – conditioned stimulus

DHA – docosahexaenoic acid

DHAPAT – Dihydroxyacetone-3-phosphate O-acyltransferase

ER – endoplasmatic reticulum

FAR – fatty acyl-CoA reductase

GABA – gamma-aminobutyric acid

GNPAT – glycerone phosphate acyltransferase

IVC – individually ventilated cage

mPTS – membrane targeting signals

PBDs – peroxisome biogenesis disorders

PEDs – single peroxisomal enzyme deficiencies

PEDS1 – plasmanylethanolamine desaturase

PEX16-AKO – adipose-specific peroxisomal biogenesis factor PEX16

PexRAP – peroxisomal reductase activating PPARgamma

PlsEtn – plasmenylethanolamine

PMP – peroxisomal membrane protein

PUFA – polyunsaturated fatty acid

RCDP – Rhizomelic chondrodysplasia punctata

RER – respiratory exchange rate

ROS – reactive oxygen species

TAE – Tris-acetate-ethylenediaminetetraacetic acid

TRAP – Total reactive antioxidant potential

US – unconditioned stimulus

USP9X – Ubiquitin-specific Protease 9X

VLCFA – very long chain fatty acids

VMAT – vesicular uptake transporter

WT – wildtype

X-ALD – X-linked adrenoleukodystrophy

ZS – Zellweger syndrome

ZSD – Zellweger syndrome disorders

1 INTRODUCTION

1.1 Peroxisomes

1.1.1. General Background

Peroxisomes as single membrane-bound metabolic organelles can be found in nearly all eukaryotic cells (Oeljeklaus et al., 2016). Peroxisomes were first discovered in 1954 in tubule cells from rodent kidneys with electron microscopy, originally described as microbodies (Rhodin, 1958). Microbodies were considered as morphological term referring to a subcellular structure enclosed by a single membrane, lacking inner membranes, surrounding a fine-grained and homogenous matrix (Rhodin, 1958). The first isolation and biochemical characterization was accomplished a decade later by Christian de Duve and Baudhuin (1966), who also introduced the term “peroxisomes” to highlight the importance of microbodies in the hydrogen peroxide metabolism (De Duve and Baudhuin, 1966). While peroxisomes were recognized as a new class of organelles at the time (late 1960s and early 1970s), they were not considered to be organelles with important functions among the majority of scientists. This has changed over the years, as the importance of peroxisomes on various metabolic processes in many different organisms including humans was gradually discovered (Vamecq et al., 2014). Nowadays it is known that peroxisomes play a vital role in the metabolism of reactive oxygen and nitrogen species, glyoxylate detoxification, in fatty acid α- and β-oxidation and ether phospholipid biosynthesis (Wanders et al., 2023).

1.1.2. Biogenesis

Peroxisome biogenesis includes the formation of peroxisomal membrane, import of peroxisomal membrane proteins (PMPs) and matrix proteins, peroxisomal growth, division, proliferation and degradation (Wanders et al., 2023).

There are different models of which peroxisomes are thought to be formed as depicted in figure 1. Peroxisomes are synthesized from pre-existing peroxisomes that grow by incorporating PMPs and matrix proteins. Followed by elongation and constriction, peroxisomes, thus, are divided by fission to form daughter peroxisomes that undergo this cycle again (Farré et al., 2019). However, peroxisomes can also be formed by *de novo* synthesis. In a specific region of the endoplasmatic reticulum (ER) called pre-peroxisomal ER some PMPs are inserted into the membrane. After insertion these regions are budded

off and form pre-peroxisomal vesicles. These vesicles then fuse to form mature peroxisomes (Farré et al., 2019).

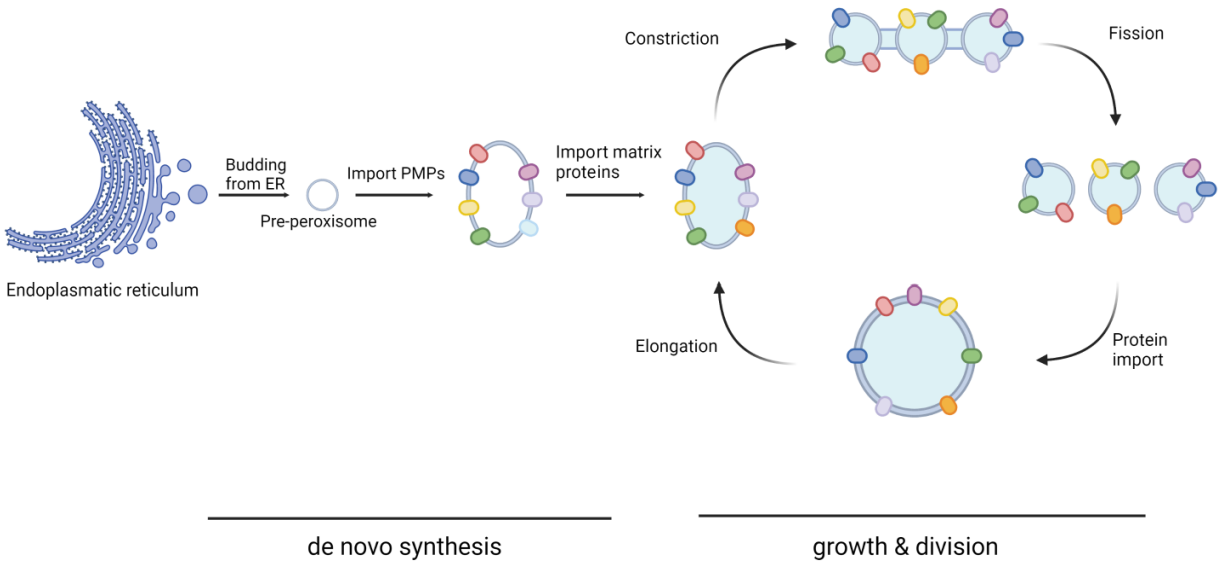

Figure 1 Schematic representation depicting two models of peroxisome biogenesis.
In the de novo pathway peroxisomes are thought to be formed by importing some PMPs into specialized regions of the ER that are then budded of forming pre-peroxisome vesicles. In the older model of growth and division peroxisomes are thought to be formed by fission of preexisting peroxisomes that undergo a process of elongation and constriction. Image created with BioRender.com, with permission, based on (Wanders et al., 2023)

All peroxisomal proteins must be imported as peroxisomes do not contain any DNA themselves (Lazarow and Fujiki, 1985). After transcription of the encoding nuclear genes and translation at free cytosolic ribosomes, they are subsequently transported to the peroxisomes. Three peroxins, namely PEX3, PEX16 and, PEX19 are essential factors for the transport and the insertion of PMPs into the peroxisomal membrane (Wanders et al., 2023). Peroxins are vital proteins for peroxisome biogenesis and are encoded by PEX genes (Waterham et al., 2016). PMPs do not carry the two peroxisomal targeting sequences PTS1 or PTS2, which are responsible for the import of proteins into the peroxisomal matrix (Jones et al., 2004).

The cytosolic protein PEX19 acts as a chaperone for newly synthesized PMPs and stabilizes them in the cytosol. Binding occurs via amino acid sequences contained in the PMPs called peroxisomal membrane targeting signals (mPTS), which are recognized by PEX19 (Jones et al., 2004). PEX19 then transports them to the peroxisomal membrane and docks with the membrane protein PEX3. PEX19-PEX3-mediated transport is called Class I pathway. Most PMPs are transported via this route. In the Class II pathway, PEX16, another peroxisomal membrane protein, acts as membrane receptor for PEX19 in complex with newly synthesized PEX3. Whether PEX16 can be considered a receptor for other PMPs remains unclear (Okumoto et al., 2020; Wanders et al., 2023).

For the transport of peroxisomal proteins from the cytosol into the peroxisomal lumen, peroxisomal matrix proteins carry one of two peroxisomal targeting signals (PTS) as shown in figure 2. Most proteins possess the C-terminal tripeptide PTS1 motif, which is recognized by the two isoforms of the cytosolic receptor PEX5 (Wanders et al., 2023). The two isoforms PEX5L and PEX5S are a result of alternative splicing of the PEX5 gene (Waterham et al., 2016). Only a small set of peroxisomal matrix proteins carry the octapeptide PTS2 motif located near the N terminus (Kunze et al., 2015). PTS2 proteins are recognized by the cytosolic receptor PEX7. PEX7 mediated transport is dependent on the co-receptor PEX5L in humans. Therefore, a defect in PEX5L causes similar consequences as a defect in PEX7 (Dorninger et al., 2017).

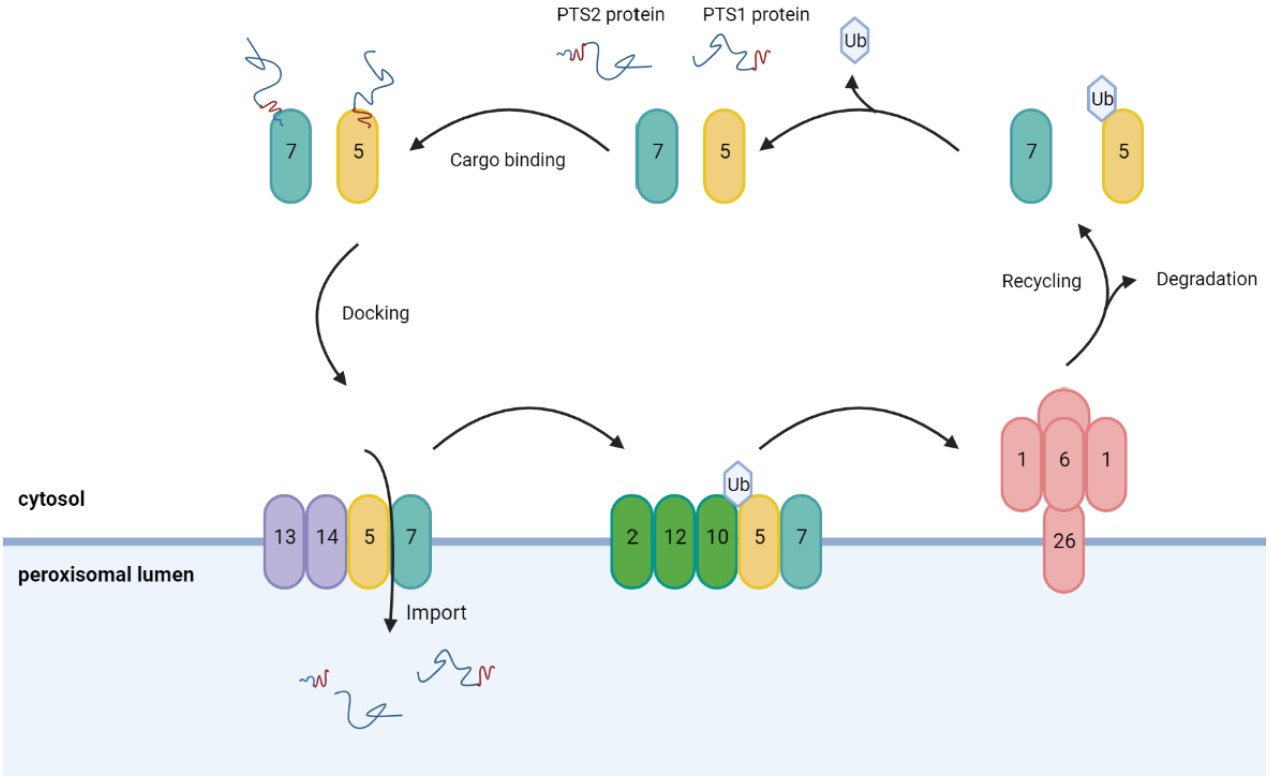

Figure 2 Schematic overview of peroxisomal matrix protein import depicting the role of the different peroxins. Peroxisomal matrix proteins containing a PTS1 or PTS2 motif are imported by PEX7 or PEX5. After unloading their cargo PEX5 and PEX7 are either recycled or determined for degradation by ubiquitination. Numbers indicate proteins from the PEX family. Image created with BioRender.com, with permission; based on (Wanders et al., 2023)

After binding of the newly synthesized proteins, the receptor/cargo complex interacts with the docking complex consisting of the peroxisomal membrane proteins PEX13 and PEX14. The matrix proteins are then imported into the peroxisomal lumen. An E3 ubiquitin ligase complex consisting of PEX2, PEX12, and PEX10 (also referred to as RING peroxins) and located in the peroxisomal membrane determines via mono- or

polyubiquitination of PEX5S/L its reuse for another import cycle or its degradation via proteasomes. Another complex in the peroxisomal membrane composed of PEX1-PEX6-PEX26 ensures the release of the monoubiquitinated PEX5S/L from the peroxisomal membrane. After deubiquitination PEX5S/L can undergo the import cycle again (Okumoto et al., 2020; Wanders et al., 2023).

Pexophagy is the autophagic process of peroxisomal degradation and can be triggered via ubiquitination or independent of ubiquitin. Ubiquitin-dependent pexophagy can be induced for example by accumulation of monoubiquitinated PEX5 at the membrane in cells with nonfunctional PEX1, PEX6 or PEX26 or by an oversupply of reactive oxygen species (ROS) leading to accumulation of monoubiquitinated PEX5 at the membrane. This oversupply induces the phosphorylation of PEX5, which in turn enhances ubiquitination of PEX5 (Wanders et al., 2023). Ubiquitin-independent pexophagy has been shown in Chinese hamster ovary (CHO) cells involving PEX14, a part of the docking complex for PEX5-mediated protein transport (Hara-Kuge and Fujiki, 2008; Jiang et al., 2015).

1.1.3. Metabolic functions of peroxisomes

Peroxisomes are found in all mammalian cell types, except for red blood cells, and are serving a variety of functions (Berger et al., 2016). One of them is peroxisomal beta-oxidation. Beta-oxidation can also take place in mitochondria, with the difference being the substrate. Beta-oxidation in mitochondria is specified for C18 and shorter fatty acids. This includes long chain, medium chain, and short chain fatty acids. Bile acid intermediates, long chain dicarboxylic, branched-chain fatty acids and very long chain fatty acids (VLCFA, C22 and above) are degraded in peroxisomes (Waterham et al., 2016). Different set of enzymes needed for fatty acid oxidation are in mitochondria and peroxisomes. But fatty acids are shortened in both cell organelles by the same catalytic mechanism of dehydrogenation, hydration, dehydrogenation, and thiolytic cleavage. However, the physiological role of peroxisomal beta-oxidation is different from its counterpart in mitochondria. Its primary purpose is not to provide energy, but to degrade its fatty acid substrates, as these are toxic when accumulated (Wanders et al., 2023; Waterham et al., 2016). Some branched-chain fatty acids with a methyl group at the 3-position like phytanic acid need to be alpha-oxidized in the peroxisomes prior to beta oxidation (Wanders et al., 2023).

Another critical function of human peroxisomes is glyoxylate detoxification. Glyoxylate is produced in the liver and converted to glycin by the peroxisomal enzyme alanine-glyoxylate aminotransferase (AGT) in both the liver and the kidneys. In the absence of AGT glyoxylate is either oxidized to oxalate by lactate dehydrogenase or reduced to glycolate. The latter can be renally secreted, however oxalate precipitates in the presence of calcium and can subsequently lead to kidney dysfunction, even kidney loss. Therefore, glyoxylates can be considered as highly toxic metabolites (Wanders et al., 2023; Waterham et al., 2016).

Peroxisomes also play a role in cellular reactive oxygen species metabolism. Several peroxisomal enzymes, such as oxidases, can generate the oxidizing H_2O_2 as by-product. At the same time, the produced H_2O_2 can be deactivated by a variety of enzymes, including glutathione peroxidase and catalase, thus creating a balance between pro-oxidant and antioxidant activity (Okumoto et al., 2020; Wanders and Waterham, 2006).

Peroxisomes are also serving a variety of functions in the central nervous system (CNS). Besides the synthesis of complex lipids such as ether phospholipids, important components of myelin, peroxisomes degrade toxic metabolites, such as phytanic acid that can damage brain structures or disrupt brain formation and D-amino acids, modulators of synaptic signaling. Furthermore, the last step of docosahexaenoic acid (DHA) is executed in the peroxisome. The very long-chain polyunsaturated fatty acid DHA is an important signaling mediator (Berger et al., 2016).

1.1.4. Peroxisomal disorders

Peroxisomal disorders can be divided into two groups: single peroxisomal enzyme/transporter deficiencies (PEDs) and peroxisome biogenesis disorders (PBDs). While PEDs only affect an individual metabolic function or pathway, PBDs lead to a loss of all or multiple peroxisomal functions due to defects in peroxisome biogenesis (Wanders et al., 2023; Waterham et al., 2016).

An important PED is X-linked adrenoleukodystrophy (X-ALD), in which a mutation in the ABCD1 gene subsequently leads to a defect in fatty acid beta-oxidation. As a consequence, VLCFA accumulate and cause a heterogeneous clinical appearance. Cerebral ALD (CALD) is a severe phenotype of X-ALD and is associated with inflammation of cerebral white matter, cerebral demyelination and severe neurological, cognitive deterioration, subsequently leading to death after two to five years of clinical symptom onset (Kemp et al., 2012; Waterham et al., 2016). Rhizomelic chondrodysplasia

punctata (RCDP) type 2-4 also belong to this group of peroxisomal disorders (Dorninger et al., 2017). RCDP is discussed in detail in section 1.2.3.

PBDs are inherited in an autosomal recessive manner and as mentioned above, result in a loss of all or multiple peroxisomal functions (Wanders et al., 2023). The largest subgroup is Zellweger spectrum disorder (ZSD) and makes up about 80% of all patients with PBDs. ZSD is subdivided into the Zellweger syndrome (ZS), the most severe form of ZSD with a clinical appearance of seizures, severe hypotonia, hepatic dysfunction and ocular abnormalities, a slightly milder neonatal adrenoleukodystrophy, and the mild infantile Refsum disease and Heimler syndrome. Patients with milder forms of ZSD exhibit a less predictable clinical course but can survive until young adulthood. Patients suffering from the severe form die within the first months after birth (Braverman et al., 2016; Fujiki et al., 2022; Wanders et al., 2023). RCDP type 1 and 5 also belongs to the group of peroxisomal biogenesis disorders and are further discussed in section 1.2.3 (Dorninger et al., 2017, p. 201).

1.2 Ether Phospholipids

1.2.1 Structure and physiological role of ether phospholipids

Phospholipids are a diverse group of lipids that are known to play an important role in both physiological and pathophysiological processes. Together with cholesterol, they are the main components of biological membranes, thereby separating cellular content from the aqueous environment and, consequently, enable formation of a variety of functional compartments with confined biochemical processes. Furthermore, they are vital for signal transduction, serving as substrates for the generation of various bioactive molecules such as diacylglycerol, lysophosphatidic acid, lysophosphatidylcholine and eicosanoids (Koivuniemi, 2017; Wang and Tontonoz, 2019).

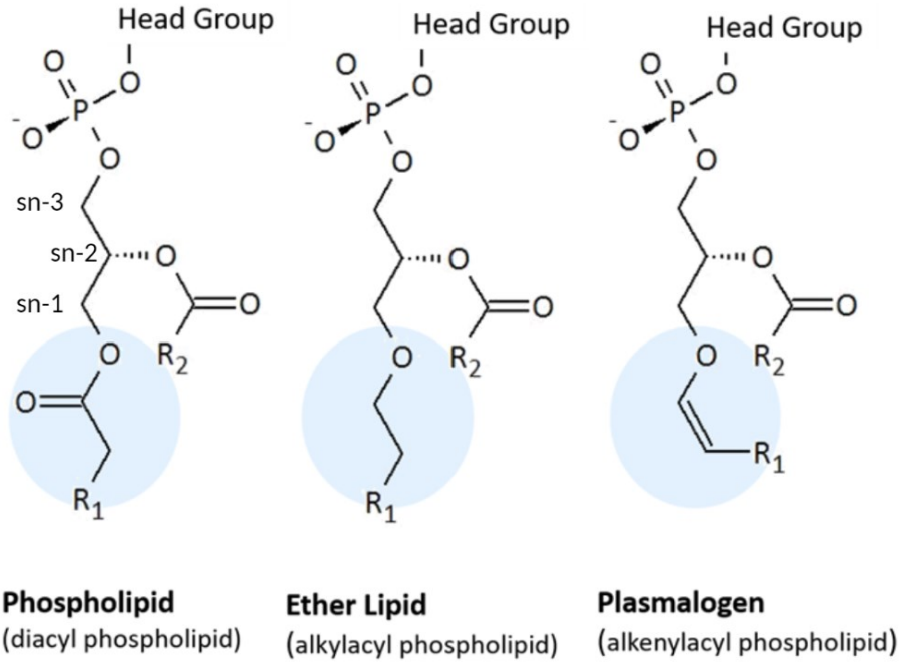

Figure 3 Chemical structure of diacyl phospholipid, ether phospholipid and plasmalogen.
Diacyl phospholipids are carrying two fatty acid residues at the sn-1 and sn-2 position. Ether phospholipids are distinguished from phospholipids by an ether bond at the sn-1 position making it an alkylacyl phospholipid. An important subgroup of ether phospholipids are vinyl ether phospholipids also known as plasmalogens or plasmenyl ether phospholipids. A cis double bond makes it a alkenylacyl phospholipid. R1 can be palmitic acid, stearic acid or oleic acid. R2 is a fatty acyl residue. The figure was drawn by Theresa König and has been slightly adapted. Used with permission from Theresa König.

Phospholipids are composed of a glycerol backbone, a hydrophilic head group and a hydrophobic tail consisting of two fatty acyl chains at the sn-1 and sn-2 position of the glycerol backbone (see figure 3). The diversity of phospholipids is among other factors due to the different chain lengths and degrees of saturation of the fatty acyl residues. This determines the biophysical properties of the membrane, which subsequently influences

processes such as signal transduction, vesical trafficking, and molecular transport (Wang and Tontonoz, 2019).

Ether phospholipids form a subgroup within the diverse group of phospholipids and can be distinguished by an ether bond at the sn-1 position of the glycerol backbone. They can be further divided into non-vinyl ether phospholipids and vinyl ether phospholipids, with the difference being a *cis* double bond adjacent to the ether bond. Both groups have been suggested to be essential for a wide variety of signaling processes with the most abundant group being the vinyl ether phospholipids, also known as plasmalogens or plasmenyl ether phospholipids, making up around 20% of the total phospholipid mass in humans (Dean and Lodhi, 2018; Dorninger et al., 2020).

Plasmalogens are particularly enriched in the brain and heart (Braverman and Moser, 2012; Nagan and Zoeller, 2001). They are thought to possess diverse functions such as protection against radicals as sacrificial antioxidants due to the vinyl ether bond, storage of essential fatty acids such as arachidonic acid and docosahexaenoic acid, which are important for brain development and cognitive processes, or signal transduction (Braverman and Moser, 2012; Dorninger et al., 2020; Nagan and Zoeller, 2001).

However, the role of plasmalogens as protective agents against oxidative stress is still topic of discussion as various experiments showing the protective ability of plasmalogens have only been carried out *in vitro* (Engelmann, 2004; Nagan and Zoeller, 2001; Sindelar et al., 1999). *In vivo* experiments in Caenorhabditis elegans have shown that ether phospholipid levels were not reduced after oxidative stress treatment, unlike phospholipids containing polyunsaturated fatty acids (Drechsler et al., 2016). In addition, in experiments with *Gnpat* KO mice (glycerone phosphate acyltransferase), a mouse model lacking all ether phospholipids (detailed description in section 1.2.4), total reactive antioxidant potential (TRAP) levels were normal (Brodde et al., 2012). Both experiments argue for a minor role of plasmalogens as antioxidants at the level of the whole organism (Wanders et al., 2023).

The role of plasmalogens as deposits of essential fatty acids, especially polyunsaturated fatty acids (PUFAs) at the sn-2 position, is more complex than initially described since other phospholipid classes are also serving as deposits for PUFAs. In a lipidomic study using fibroblasts from RCDP patients (a disease causing ether phospholipid deficiency - see section 1.2.3) and brain tissue from plasmalogen deficient mice, it was shown that the total amount of PUFAs was maintained, although plasmalogens were absent. PUFAs were shifted to phosphatidylethanolamines. Even though, the total amount of PUFAs was

preserved, the balance between ω-6 and ω-3 fatty acids was disturbed, possibly leading to long-term physiological consequences (Dorninger et al., 2015). Docosahexaenoic acid (DHA) and arachidonic acid (AA) as the main representatives of ω-3 and ω-6 fatty acids promote a variety of essential biological processes. AA is a precursor of many proinflammatory mediators such as leukotrienes, prostaglandins and thromboxanes, whereas DHA acts as the anti-inflammatory counterpart. Therefore, plasmalogens as one source of these fatty acids are crucial for providing important signaling mediators (Dorninger et al., 2020).

The contribution of ether phospholipids, especially plasmalogens for membrane composition, is known to affect a variety of signaling pathways (Dorninger et al., 2020). Due to the biophysical properties plasmalogens provide selective structural and dynamical properties for biomembranes. For example, plasmenyl ethanolamine (PlsEtn), a plasmalogen with ethanolamine as head group, is known to stabilize hexagonal nonlamellar structures (Lohner et al., 1991). This suggests an important role of PlsEtn in membrane fusion and fission, crucial processes for synaptic vesicle cycle (Dorninger et al., 2017; Jiménez-Rojo and Riezman, 2019; Wanders et al., 2023). Accordingly, vesicles containing PlsEtn fuse more rapidly than vesicles with phosphatidylethanolamine (Glaser and Gross, 1994). Membranes and vesicles with PlsEtn have demonstrated reduced surface tension, another possible factor of how plasmalogens are influencing endo- and exocytosis processes (Rüdiger et al., 1998). In accordance with this, it was shown that in both synaptic membranes and in synaptic vesicles plasmalogens are major constituents (Hofteig et al., 1985; Takamori et al., 2006). Plasmalogens are also enriched in lipid rafts (or membrane rafts), specialized membrane domains that compartmentalize cellular processes, including cell signaling (Pike, 2006; Pike et al., 2002, p. 200). The impact on signaling pathways was shown by Rubio et al. (2018) (Rubio et al., 2018). In their experiment with plasmalogen deficient macrophages phagocytosis was decreased due to changes in formation, fluidity and functioning of the plasma membrane of membrane rafts. Another example of the influence of ether phospholipids on signaling pathways was demonstrated by Brites (da Silva et al., 2014). Lack of plasmalogens in *Gnpat* KO mice resulted in impaired recruitment and phosphorylation of protein kinase B, changing downstream signaling processes subsequently leading to defects in myelination (da Silva et al., 2014). In experiments using a mouse model, in which *Gnpat* mRNA was targeted by lentiviral shRNAs causing downregulation of plasmalogen synthesis, a link between plasmalogen levels and another signaling cascade involving mitogen-activated protein

kinase ERK was established. Injection of the shRNA caused reduced phosphorylation of ERK in the cerebral cortex and increased microglial activation promoting a proinflammatory state (Hossain et al., 2017). In addition, several *in vitro* experiments have shown plasmalogen supplementation attenuates the proinflammatory state of microglial cells (Ali et al., 2019; Youssef et al., 2019). If plasmalogen supplementation also has *in vivo* relevance remains to be seen (Dorninger et al., 2020).

An interesting connection between the role of plasmalogens and mitochondrial membrane dynamics has been recently suggested by Park et al. (2019) (Park et al., 2019). Knockout of the GNPAT gene in mice resulted in decreased mitochondrial copy number and mitochondrial dysfunction. The same outcome was observed by knocking out adipose-specific peroxisomal biogenesis factor PEX16 (PEX16-AKO) in mice. Plasmalogen supplementation in PEX16-AKO mice attenuated the negative effects on mitochondrial copy number and function (Park et al., 2019).

1.2.2 Biosynthesis of ether phospholipids and plasmalogens

The biosynthesis of ether phospholipids as well as plasmalogens is a multistep process involving a variety of cell organelles as shown in figure 4. The peroxisome plays a crucial role, as the initial steps of the synthesis, the formation of the characteristic ether bond, is carried out there. Two peroxisomal membrane-bound enzymes are responsible for this step: Dihydroxyacetone-3-phosphate-O-acyltransferase (DHAPAT; encoded by the gene: glycerone phosphate acyltransferase, GNPAT) and alkyl-dihydroxyacetone phosphate synthase (ADHAPS; encoded by the gene: alkylglycerone phosphate synthase, AGPS). DHAPAT catalyzes the transfer of a fatty acid to the sn-1 position of dihydroxyacetone-3-phosphate generating 1-acyl-dihydroxyacetone-3-phosphate. For the second step, the reaction catalyzed by the enzyme ADHAPS, a fatty alcohol is needed. The fatty alcohol is supplied by fatty acyl-CoA reductase (FAR), a COOH tail-anchored protein with its catalytic site exposed to the cytosol (Dorninger et al., 2017; Wanders et al., 2023). This step has been suggested to be rate limiting in plasmalogen biosynthesis due to feedback mechanisms promoting instability of FAR1, one of two variants of FAR, when sensing plasmalogens in the inner leaflets of the plasma membrane (Honsho and Fujiki, 2017). The generated fatty alcohol and 1-acyl-DHAP are substrates for ADHAPS that catalyzes the reaction resulting in the generation of the ether bond. It was previously thought that the generated 1-O-alkyl-DHAP is then shuttled across the peroxisomal membrane, where the enzyme acyl/alkyl-dihydroxyacetone-3-phosphate

reductase (ADHAPR, encoded by the gene: peroxisomal reductase activating PPARgamma, PexRAP) reduces the ketone at the sn-2 position creating 1-O-alkyl-glycerol-3-phosphate (1-O-alkyl-G3P). However, ADHAPR was also found in the ER. Recent findings suggest that the ER version of ADHAPR is responsible for catalyzing this step (Dorninger et al., 2017; Wanders et al., 2023). All subsequent steps for the biosynthesis are executed in different cell compartments, depending on the type of ether phospholipid (Dorninger et al., 2020).

The final steps of plasmalogen biosynthesis are carried out at the ER, where the plasmanyl ethanolamine desaturase (*Peds1*; encoded by the gene: TMEM189) introduces the characteristic alk-1-enyl ether double bound, resulting in the creation of plasmalogens, or more precisely plasmenyl ethanolamines. Plasmenyl cholines, plasmalogens carrying a choline as head group, are synthesized from plasmenyl ethanolamines, as they are not substrates of *Peds1* (Werner et al., 2020).

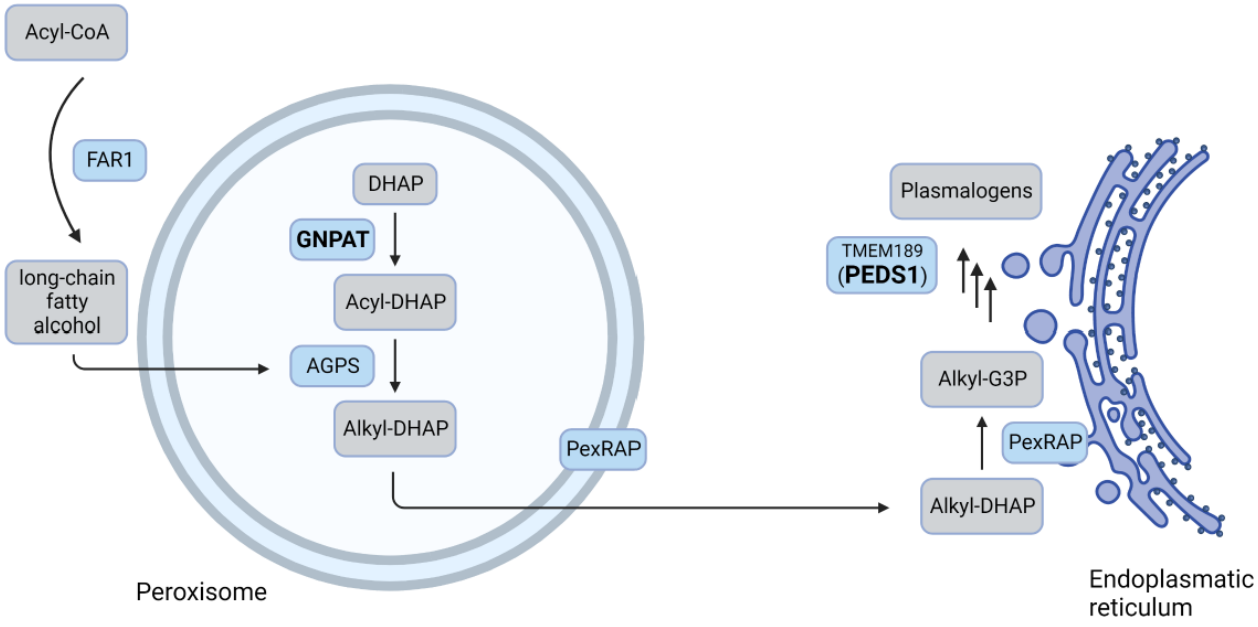

Figure 4 Plasmalogen biosynthesis.
Graph shows a simplified version of the initial steps of ether phospholipid biosynthesis in the peroxisome and the final steps of plasmalogen biosynthesis at the ER. Blue boxes indicate the genes encoding for the catalyzing enzymes, with the exception of *Peds1*, which is the enzyme name. Image created with BioRender.com, with permission; based on (Werner et al., 2020; Wanders et al., 2023)

1.2.3 Rhizomelic chondrodysplasia punctata

Rhizomelic chondrodysplasia punctata is an inherited and fatal metabolic disease characterized by ether phospholipid synthesis defects and impaired peroxisomal functions. RCDP is inherited in an autosomal recessive fashion with an incidence of 1 in

100 000 live births (Duker et al., 2017; Stoll et al., 2008). There are 5 types of the disease, depending on which gene in the biosynthesis process is affected. Type 1, the most common subtype, is caused by a mutation in the PEX7 gene causing a defect in the cytosolic receptor protein PEX7, responsible for binding peroxisomal proteins containing a PTS2 motif. Subsequently, the enzyme ADHAPS is not imported leading to a loss of peroxisomal function. In type 2 (mutation in the GNPAT gene leads to a defective DHAPAT enzyme) and type 3 (mutation in the AGPS gene leads to a nonfunctional ADHAPS enzyme), only the two enzymes responsible for initiating ether phospholipid biosynthesis are defective. In RCDP type 4 a lack of long-chain fatty alcohols needed for ether phospholipid synthesis is caused by a mutation in the FAR1 gene. In type 5, a mutation in the PEX5 gene results in loss of PEX5L function. PEX5L is required as co-receptor for PEX7-mediated peroxisomal protein transport. Without PEX5L, PEX-7-mediated transport for proteins carrying the PTS2 motif is not possible. This leads similar consequences to those of RCDP type 1 (Dorninger et al., 2017; Duker et al., 2020). RCDP type 5, like type 1, belongs to peroxisomal biogenesis disorders that result in loss of several or all peroxisomal functions, whereas types 2-4 are single peroxisomal enzyme deficiencies (Wanders et al., 2023; Waterham et al., 2016).

In RCDP patients, an impaired ether phospholipid biosynthesis causes a loss of all or at least a reduction in ether phospholipids. Absence of ether phospholipids leads to a variety of severe pathological changes, including mental and physical developmental defects, shortened proximal limbs (rhizomelia), calcification of joints (chondrodysplasia punctata), cerebral and cerebellar atrophy, myelination defects, and respiratory difficulties, often resulting in early death within the first decade of life (Braverman et al., 2001; Kou et al., 2011). Patients with RCDP type 1,2,3, and 5 show the same clinical appearance and cannot be distinguished from each other based on their symptoms. Only patients with RCDP type 4 can be distinguished by an absence of rhizomelia. In addition to the severe form of RCDP, the disease can take an attenuated course (nonclassic RCDP), which correlates with residual activity of the affected enzymes. Patients with the milder course are still severely impaired but can at least reach young adulthood. Most patients with mild RCDP show clinical features such as multiple calcifications of joints, impaired developmental growth and bilateral cataracts (Braverman et al., 2001). Some RCDP cases have reported patients with the milder form that were diagnosed with autism and attention deficit hyperactivity disorder, suggesting a possible link between ether phospholipid deficiency and neurodevelopmental disorders. A reported genetic

association between PEX7 and attention deficit disorder as well as findings of reduced levels of plasmalogens in red blood cells and plasma of autistic patients underline the connection between ether phospholipid deficiency and neurodevelopmental disorders (Berger et al., 2016; Yu et al., 2013).

Treatment for patients with the severe (classic) form of RCDP is limited to supportive therapy due to the poor outcome and severity of the multiple impairments. Control of respiratory function, feeding therapy, adequate anti-seizure medication, cataract extraction for preservation of vision are examples of treatment options that may be required. In patients with the mild form of the disease, surgical interventions are recommended to preserve mobility (Braverman et al., 2001).

1.2.4 *Gnpat* KO mouse

To draw conclusions about the functions of ether phospholipids or the role of plasmalogens in the human body and in order to understand the pathophysiology of RCDP in detail, suitable mouse models were generated by disrupting exons 5-7 of the GNPAT gene. The *Gnpat* KO mouse (official mouse line name: B6.129-Gnpat^{tm1Just}) was first described in 2003 (Rodemer et al., 2003). Loss of the GNPAT gene results in a complete absence of ether phospholipids. Phenotypically, the symptoms resemble the human disease RCDP, although the clinical appearance seems to be less severe in mice than in human (Gorgas et al., 2006). *Gnpat* KO mice are largely viable (provided they survive a critical period in the first month of life), but they exhibit various abnormalities: In general, males are infertile, they exhibit growth deficits, structural defects in the eye and brain, incomplete myelination, and altered cellular membrane composition (Rodemer et al., 2003; Gorgas et al., 2006; Komljenovic et al., 2009; Teigler et al., 2009). *Gnpat* KO mice lead a normal life despite mild physical impairments (mainly visual impairment and reduced growth) until the age of about one year; thereafter increased motor impairments can occur.

Disturbed neurotransmitter homeostasis in *Gnpat* KO mice was shown by Dorninger et al. (2019b). Decreased levels of the monoamine neurotransmitters serotonin, norepinephrine and dopamine were found by HPLC analysis of homogenates from the cerebrum. The inhibitory neurotransmitter GABA (gamma-aminobutyric acid) was also reduced in *Gnpat* KO mice compared to their wildtype (WT) littermates. In further experiments, GABA levels were also reduced in parietal cortex and substantia nigra but not striatum, all three brain regions rich in GABAergic synapses. A loss of synapses did

not account for the reduced neurotransmitter levels as western blot analysis of synaptic marker proteins showed no alteration between the genotypes. In accordance with the reduced neurotransmitter levels, neurotransmitter release upon high-intensity stimulation using brain slices from hippocampus and parietal cortex of *Gnpat* KO and WT controls was found to be impaired. Response to low-intensity stimulation was adequate. Alternating levels of proteins involved in the neurotransmitter cycle were suggested to accompany changes in neurotransmitter levels and release, but only a reduction in norepinephrine transporter was found. Dopamine transporter, NMDA transporter and serotonin transporter were not affected in *Gnpat* KO mice. Levels of vesicular uptake transporter VMAT2 were reduced in the striatum of *Gnpat* KO mice compared to their WT controls suggesting VMAT2 deficiency as the limiting factor for neurotransmitter transport into the synaptic vesicles, subsequently leading to depletion of monoamine neurotransmitters (Dorninger et al., 2019b). Disturbed neurotransmitter homeostasis in *Gnpat* KO mice is manifesting in a complex behavioral phenotype mimicking certain aspects of human psychiatric disorders, particularly autism and attention-deficit hyperactivity disorder (Dorninger et al., 2019a).

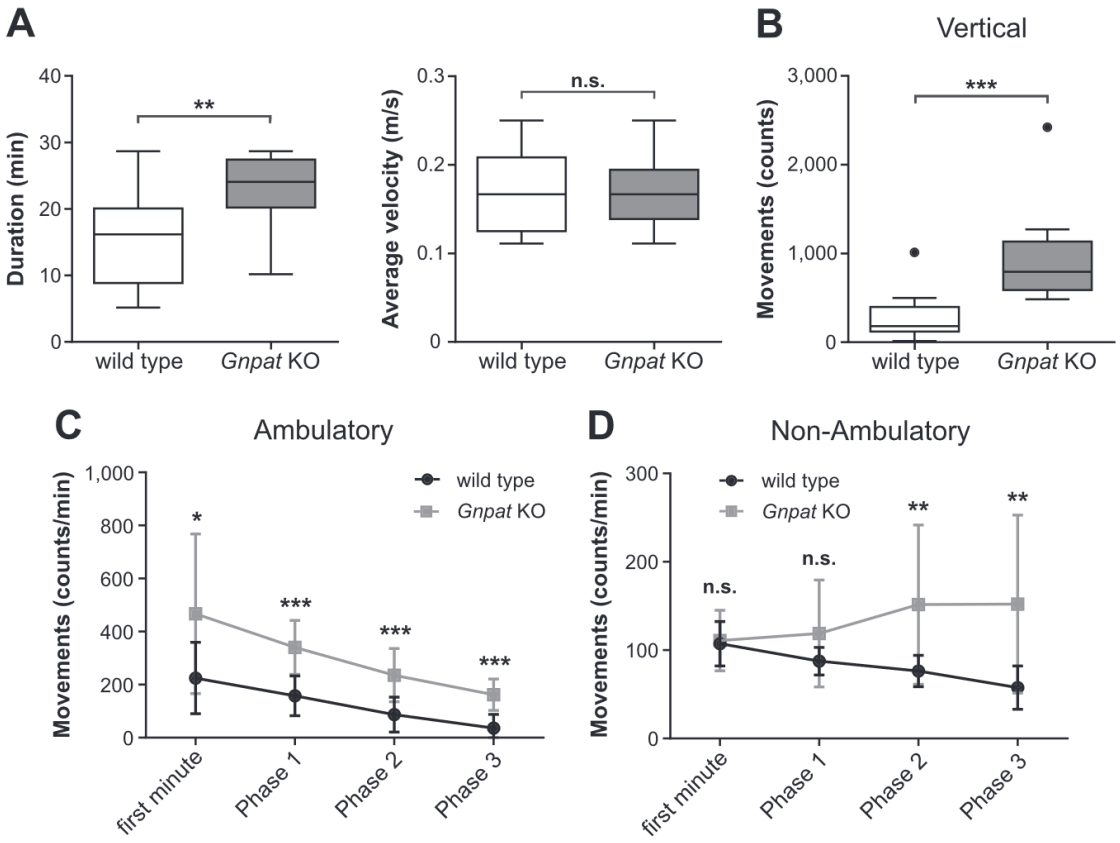

Figure 5 Closed-wheel task and three-chamber social interaction task of *Gnpat* KO mice vs WT controls. (A) Results of closed-wheel task are presented as average velocity (right graph) and time active (left graph) during a 30-min trial. Cohort consisted of *Gnpat* KO n=11; WT Controls n=13. Two-tailed Student's t-tests were used for statistical analysis. Box plots (A) & (B) are drawn via Tukey's method with whiskers reaching to the highest value within the 75th percentile plus 1.5 times the interquartile range and to the lowest value within the 25th percentile minus 1.5 times the interquartile range. (B) (C) and (D) are showing results of the open field test of the same cohort, a paradigm assessing locomotor activity. Trial was 61 min long, with the first minute separated and used as indicator for exploratory behavior. Remaining time was split into phase 1: minute 2-21, phase 2: minute 22-41 and phase 3: minute 42-61. Mann-Whitney U-test was used for statistical analysis of the boxplot (B). Results in (C) & (D) are presented as mean ± SD with (C) showing counts/min of ambulatory movement and (D) counts/min of non-ambulatory movement. Two-tailed Student's t-tests was used for statistical analysis followed by Holm-Sidak correction for multiple testing. $***$ $P < 0.001$; $**$ $P < 0.01$; $*$ $P < 0.05$; n.s., not significant. Figure from (Dorninger et al., 2019b) used with permission.

In a closed-wheel task (see figure 5 A), where mice were presented with either the option to run or to rest, *Gnpat* KO mice chose to spend more time running in comparison to their WT littermates with similar speed. In an open field test, a paradigm for measuring locomotor activity, movement in all categories (vertical, ambulatory and non-ambulatory) of *Gnpat* KO mice was higher than of their WT controls indicating hyperactivity in *Gnpat* KO mice (see figure 5 (B), (C), (D)). Ambulatory activity is defined as forward moving motion, while non-ambulatory movement includes movement like grooming. Vertical activity mainly represents rearing. The first minute was separated as it indicates exploratory behavior and not locomotor activity. Although in both WT controls and *Gnpat* KO mice ambulatory movement was decreased with time, ambulatory movement was still

higher in *Gnpat* KO mice than in WT controls. On the contrary, non-ambulatory movement was increased in *Gnpat* KO mice during the trial, whereas it lowered in WT controls (Dorninger et al., 2019b).

Further behavioral experiments on male *Gnpat* KO mice revealed more behavioral abnormalities (Dorninger et al., 2019a). Social interaction was assessed using a three-chamber arena, in which social interaction was defined as percentage of time a subject mouse has spent in direct contact with another unfamiliar stranger mouse (matched in age and sex) compared to a novel object. For this trial, a contact zone around the retainer with the stranger mouse and the object was defined. Although both *Gnpat* KO mice and WT controls were showing a preference for the stranger mouse, the preference for the stranger was reduced in *Gnpat* KO mice compared to their WT controls as shown in figure 6. In this setting, the percentage of time spent in direct contact with the stranger or object was used as a parameter for social interaction. With regard to the results from Dorninger and colleagues showing impaired marble burying and nestlet shredding in *Gnpat* KO mice, it was suggested that *Gnpat* KO mice display difficulties performing inborn behavioral patterns (Dorninger et al., 2019a).

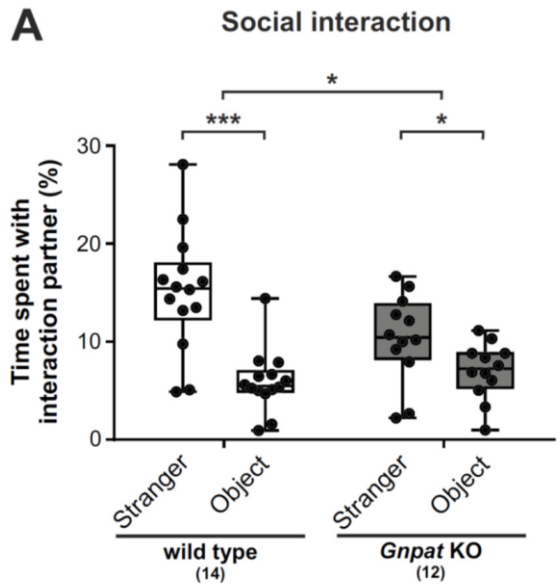

Figure 6 Social Interaction was performed in a three-chamber arena.
(A) Social interaction was defined as percentage of time spent in direct contact with interaction partner. For this a contact zone around the retainer containing the stranger mouse or the novel object was defined. Data are presented as boxplots with individual data points, whiskers indicate minimum and maximum values. For the comparison of the preference within each genotype a two-tailed Student's t-test was used for statistical analysis. Repeated measurements of two-way ANOVA were performed for comparison of the genotypes. *** $P < 0.001$; * $P < 0.05$. Figure from (Dorninger et al., 2019a) used with permission.

Furthermore, it was shown that *Gnpat* KO mice displayed reduced freezing response in contextual and cued fear conditioning as shown in figure 7. Fear conditioning is an

associative learning task in which mice learn to associate a conditional stimulus (CS, tone) with an unpleasant unconditional stimulus (US, mild electric foot shock). After repeated presentations of both US and CS, wildtype mice react by freezing when presented the same context or tone. Reduction of freezing response in *Gnpat* KO mice compared to their WT counterparts suggests memory deficits (Dorninger et al., 2019a).

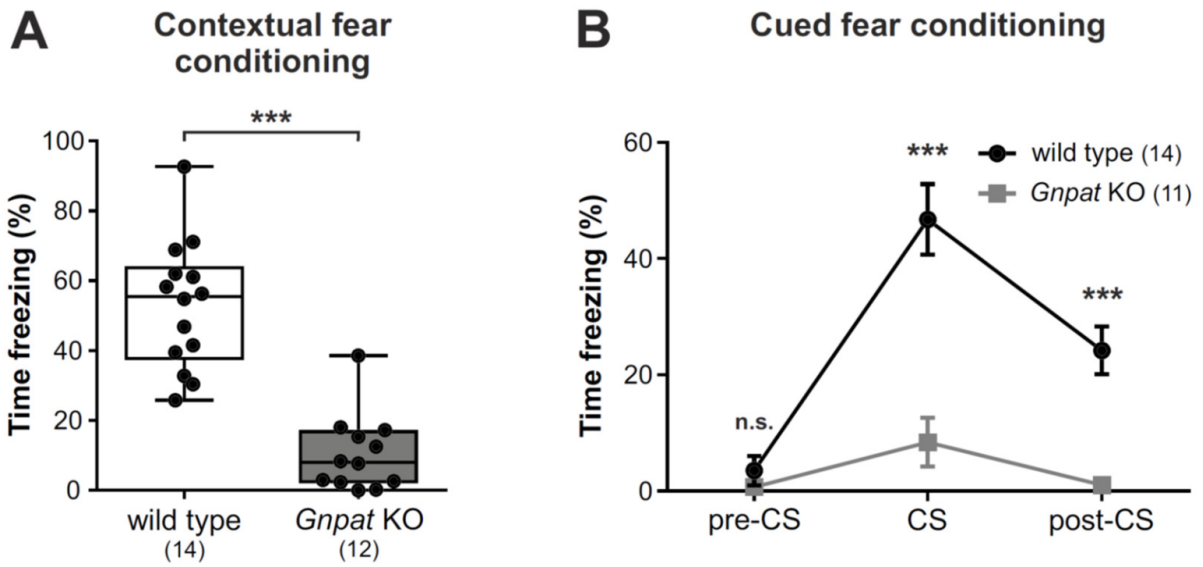

Figure 7 Contextual and Cued fear conditioning on *Gnpat* KO vs WT controls.
Gnpat KO mice show in both tests a significant reduction in freezing response compared to their WT controls. (A) Contextual fear conditioning was tested 24h after training session by placing testing mouse in the same testing environment without US or CS presentation. Data are presented as boxplot with individual data points, whiskers indicating maximum and minimum values. Two-tailed Student's t-test was used for statistical analysis. (B) Cued fear conditioning was performed 3 hours after contextual fear conditioning trial by placing the mouse in a different modified fear conditioning box with a single CS presentation. Freezing time was quantified before (pre-CS), during (CS) and after (post-CS) conditioned stimulus presentation. Data are presented as mean ± SEM. Mann-Whitney U tests with Bonferroni correction for multiple testing were used for statistical analysis. *** $P < 0.001$; n.s., not significant. Figure from (Dorninger et al., 2019a) used with permission.

In addition, in paradigms assessing anxiety-related behavior (light/dark box, novelty-suppressed feeding test, elevated plus maze) alterations in *Gnpat* KO mice were found. In the forced swim test, in which depression like behavior is characterized by immobility of mice when placed into a beaker filled with water and without the possibility of escape, *Gnpat* KO mice have shown higher freezing responses than their WT controls. In contrast, the tail suspension test, another paradigm relevant for depression-like behavior, revealed no differences between the genotypes in freezing response (Dorninger et al., 2019a).

1.2.5 *Peds1*-deficient mouse

The gene Tmem189 encodes the enzyme plasmanyl ethanolamine desaturase (*Peds1*) that catalyzes the generation of the vinyl ether double bond at the sn-1 position of plasmanyl ethanolamine, the characteristic structural feature of plasmalogens (Werner et al., 2020). Insertion of ß-galactosidase in the PEDS gene causes a complete loss of function of the enzyme, thus creating a *Peds1*-deficient mouse model (official mouse line name: $Tmem189^{tm1a(KOMP)Wtsi\ tg/tg}$). For simplification *Peds1*-deficient mice will be referred to as *Peds1* KO mice. Without functioning *Peds1* enzymes, the last step required for plasmalogen synthesis is inhibited, subsequently leading to a loss of plasmalogens (Werner et al., 2020). In contrast to *Gnpat* KO mice that lack all ether phospholipids, the synthesis of non-vinyl ether phospholipids in *Peds1*-deficient mice is still enabled. It was shown that absence of plasmenyl ethanolamine lead to an equal rise in plasmanyl ethanolamine, one of many changes in lipidome composition in a variety of tissues (Lackner et al., 2023).

Phenotypic abnormalities characterized by the European Mouse Mutant Archive (EMMA) include reduced lean body mass, abnormalities in the hematopoietic and skeletal system as well as in the eyes (Lackner et al., 2023). Accordingly, it was previously shown that *Peds1*-deficient pups have lower body weights compared to their WT controls at time of weaning (Werner et al., 2020). So far, no behavioral experiments have been conducted on *Peds1*-deficient mice. We therefore wanted to study the effect of vinyl ether and non-vinyl ether phospholipids on mouse behavior in greater detail.

1.3 Aims of the Study

Ether phospholipids, especially plasmalogens, are of vital importance to a variety of processes and functions in the brain (Berger et al., 2016; Braverman and Moser, 2012). A disturbance in neurotransmitter homeostasis as well as a complex behavioral phenotype mimicking certain aspects of human psychiatric disorders in *Gnpat* KO mice was a clear result of a lack of ether phospholipids (Dorninger et al., 2019b, 2019a). Our hypothesis states that the neurological phenotype of *Gnpat* KO mice is firstly caused by an absence of non-vinyl ether phospholipid mediators and secondly due to altered membrane properties as consequence of the lack of plasmalogens. As *Peds1* KO mice do not lack in non-vinyl ether phospholipids but in plasmalogens we expected a different behavioral phenotype in *Peds1* KO mice compared to *Gnpat* KO mice as well as WT controls.

The aim of this study was to elucidate the physiological role of non-vinyl as well as vinyl-ether phospholipids on mouse behavior, by performing a variety of different behavioral assays with both *Gnpat* KO mice and, *Peds1* KO mice as well as WT littermates as controls, with one lacking all ether phospholipids, one lacking only vinyl-ether phospholipids and the controls not lacking any phospholipids, respectively.

2 MATERIALS AND METHODS

2.1. Animals

2.1.1. Mice cohort

All experiments were performed with male and female *Gnpat* KO, *Peds1* KO mice as well as sex- and age-matched WT controls, when possible from the same litter and, between the age of 3 to 5 months. Littermates were obtained by mating heterozygous animals. *Peds1* KO mice previously kept on an outbred C57BL/6 background were backcrossed at least 5 generations into the genetic background of the *Gnpat* KO mice (outbred C57BL/6 x CD1), resulting in the same genetic background in all used groups. All genotypes were determined by PCR either in toe clip genomic DNA taken 4 to 8 days after birth or in ear notch genomic DNA taken at weaning and confirmed at death using tail clips. Two *Peds1* KO female mice were excluded from all experiments due to the fact that one animal was mixed up with a heterozygous animal in the same cage and was accidentally killed before the start of the experiments. The second animal was determined as heterozygous animal after retyping of the genotype after death.

Table 1 Overview of animal cohort used for behavioral experiments. Animals excluded from all experiments are not included in the table.

	n	Male	Female	Age at the start of experiments [m]
***Gnpat* KO**	12	6	6	3,4 (± 0,9)
***Peds1* KO**	10	7	3	3,3 (± 0,5)
WT Controls	12	6	6	3,4 (± 0,9)

2.1.2. Ethical considerations

In all experiments, care was taken to adhere to the 3R principles (replacement, reduction, refinement). Experiments in human fibroblasts on the effects of ether lipid deficiency on mammalian cell phospholipid composition and further *in vitro* experiments preceded the animal experiments (replacement) (Dorninger et al., 2015). To investigate the physiological role of non-vinyl ether phospholipids and vinyl ether phospholipids on mouse behavior, *in vitro* experiments cannot be replaced but are in the position to complement experiments on the living mammalian organism. Precise statistical calculations were carried out to estimate the minimum required animals to obtain clear-

cut and, statistically significant results. Standardization of experimental protocols (same time of day, light conditions, etc.), sufficient time for habituation, as well as different materials in the cages for enrichment, were measures to minimize stress for the animals (refinement). All experiments were approved by the Austrian Federal Ministry of Education, Science and Research (BMBWF-66.009/0174-V/3b/2019; BMBWF-GZ2021-0/451.840; BMBWF-GZ2023-0.088.476).

2.1.3. Determination of mouse genotype

For determination of the genotype toe clips taken 4 to 8 days after birth or ear clips taken 21 days after birth were used. For lysis and PCR KAPA HotStart Mouse Genotyping Kit K7352 (Kapa Biosystems, Inc.) was used. Each DNA sample was lysed in 100 µL lysis mix consisting of 88 µL PCR grade water, 10 µL 10x KAPA Express Extract Buffer and 2 µL KAPA Express Extract Enzyme. The DNA samples in lysis mix were heated at 75°C for ten minutes for lysis, then for 5 minutes at 95°C for inactivation of the enzyme. The sample mix was kept at 4°C until PCR analysis.

For determination of genotype of *Gnpat* mice a PCR master mix was prepared by mixing 10 µL 2x KAPA2G fast Genotyping Mix with dye, 0,8 µL Oli 1626 (10 µM), 1,0 µL Oli 1627 (10 µM), 0,8 µL Oli 1628 (10 µM), 6,4 µL PCR grade water per DNA sample and pipetted into PCR tubes. For samples from *Peds1* mice a different PCR master mix was used containing 10 µL 2x KAPA2G fast Genotyping Mix with dye, 0,5 µL Oli 2825 (10 µM), 1,0 µL Oli 2826 (10 µM), 0,5 µL Oli 2827 (10 µM), 6,4 µL PCR grade water per DNA sample. 1 µL of DNA was added to the PCR master mix amounting to a total volume of 20 µL per DNA sample in the PCR tubes. The following PCR program was used for both samples from *Gnpat* and *Peds1* mice. One minute of initial denaturation at 94°C was followed by 35 cycles of 94°C for 20 s, 60°C for 20 s and 72°C for 50 s. Afterwards samples were cooled down to 72°C for 7 minutes and then cooled further down to 4°C until gel electrophoresis. For gel electrophoresis a 1.5% agarose gel containing 0.5 µg/mL ethidium bromide was used. The gel was bedded in Tris-acetate-ethylenediaminetetraacetic acid (TAE) buffer (1 mM EDTA, 40 mM Tris-acetate, pH 8.0). Samples were applied into gel pockets and electrophoresis was performed for about 1 h at 100 mV. For visualization of DNA bands Gel Doc 2000 gel documentation system (Bio-Rad) and the Bio-Rad software were used.

For determination of the genotype of *Gnpat* mice fragments for wildtype allele were 700 base pairs in length and for the knockout allele 900 base pairs in length. In samples from

Peds1 mice fragments for the wildtype allele were 411 base pairs in length and for the knockout allele 223 base pairs in length.
For confirmation of genotype using DNA in tail clips the same protocol was used.

2.1.4. Housing conditions

All animals were bred at the core facility for laboratory animal breeding and husbandry (CFL) of the Medical University of Vienna under controlled, standardized optimal hygienic conditions with an artificial day-night rhythm of 12:12 h with standard chow (LasVendi or Altromin breeding or husbandry mouse feed) and water *ad libitum*. Room temperature was maintained at 22±2°C and humidity at 55±10%. The animals were kept in conventional polysulfone type IIL cages in groups of up to 5 animals (littermates) and were checked at least once a day by the animal caretakers of the CFL. Cages were littered with aspen wood bedding (LASbedding PG2, LASvendi Company, Germany) and contained nesting material (sizzlenest, LASvendi) as well as nail timbers (Tapvei S-Bricks, Aspen Enrichment, Estonia) for enrichment.
The behavioral experiments were conducted in the Preclinical Phenotyping Facility at the Vienna Biocenter Core Facilities GmbH (VBCF), member of Vienna Biocenter (VBC), Austria. Animals were transported 2 weeks prior start of the experiments for the mice to adjust to the new environment. They were kept on an artificial day-night rhythm of 14:10 h with lights turned on at 6 am and switched off at 8 pm. Room temperature was maintained at 22±1°C and humidity at 55±5%. In the animal room (not in the testing rooms), muffled music (white noise) was broadcast through loudspeakers at a level of 40-45 dB, providing a continuous moderate noise level as protection against the negative effects of unexpected and sudden noise. Movable polycarbonate, polyester carbonate and polysulfone containers with transparent fixed bottoms and side walls were used as cages with up to 5 mice per cage. An IVC (individually ventilated cage) hood ensured isolation of the caged animals from the environment. Absorbent aspen wood bedding (ABEDD, Germany) was changed once a week by professional animal caretakers. In case of overlap with experiments, this was done after the experiment when body weight was checked. Mice were fed standard chow (SSNIFF, Germany) and acidified, steam-sterilized water (pH 2.5-3.0; for minimization of the risk of infection) *ad libitum*.

2.1.5. Testing conditions

All experiments were conducted in separate testing rooms from 9 am to 5 pm. Males and females were tested separately starting with the males. One day prior to the start of the first experiment the group housed animals were labelled by drawing up to four circles around the tails for simpler identification during the testing day. Labels were redrawn every other day until single housing. Before the start of any experiment mice were given at least 30 minutes to adjust to the testing room. After the experiment body weight was measured for monitoring wellbeing.

2.2 Experimental outline and statistical analysis

The first experiment conducted was social interaction lasting two days (habituation and test). Before the start of the metabolic cage, two more experiments which were not part of this thesis were conducted. Afterwards, mice were single housed for a week, then put in the metabolic cage for 8 days. Wellbeing of the mice was checked once a day. A three-day fear conditioning trial was performed as last experiment to prevent possible trauma from the trial influencing the results of the other behavioral experiments. Taken together, all experiments were conducted in 23 days.

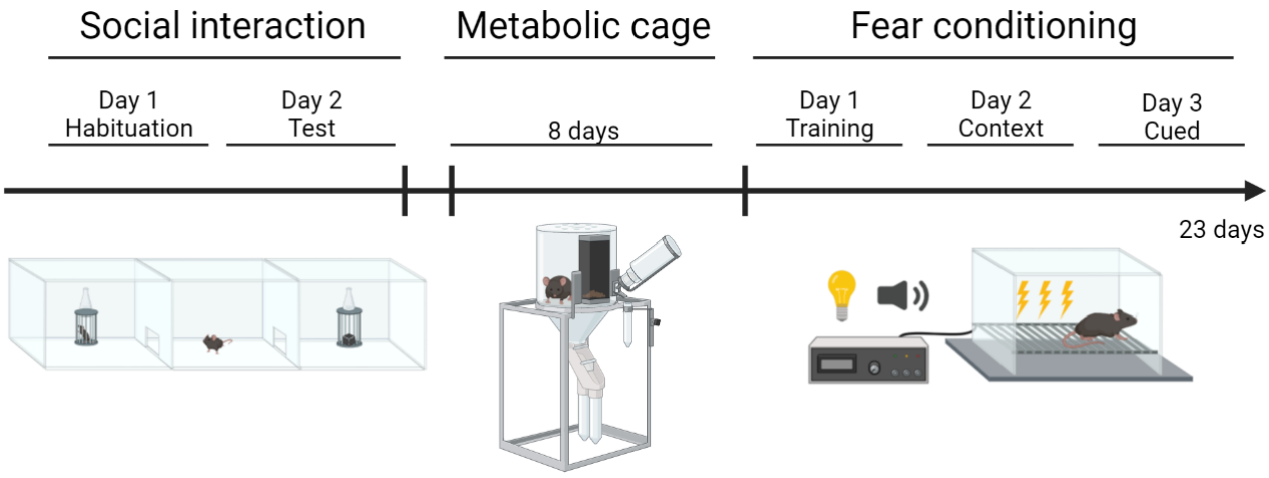

Figure 8 Experimental outline including social interaction, metabolic cage and fear conditioining.
Behavioral assays not part of this thesis were left out. Social interaction was conducted first, fear conditioning last and the metabolic cage in between. All trials were conducted in a 23-day period. Image created with BioRender.com, with permission.

Details on the exact statistical procedure are provided in the figure legends. Statistical analysis is indicated with **** $P < 0.0001$; *** $P < 0.001$; ** $P < 0.01$; * $P < 0.05$; n.s., not significant. Depicted in box plots, the box is extending from the 25th to 75th percentiles, with whiskers indicating the smallest and largest values. Line graphs for parameters from

the metabolic cage were drawn for better visualization and were not statistically analyzed. Drawing of graphs and statistical calculations were performed using GraphPad Prism version 9.5.1 for Windows (GraphPad Software, San Diego, California USA, www.graphpad.com)

2.1.6. Social Interaction

Social interaction was conducted in a three-chamber arena built in an IMP-IMBA scientific workshop using the video tracking software “Topscan” (Cleversys, Inc.; USA) following an adapted and, previously published protocol by Nadler (2004) (Nadler et al., 2004). In comparison to this protocol which used an empty retainer as novel object, a black object about the size of a mouse was put in the retainers in our experiments. In addition, 10 minutes for habituation and 5 minutes for the test were used, instead of 5 minutes for habituation and 10 minutes for the test established in the protocol, respectively.
The three-chamber arena was placed under a connected camera and moved until the chamber walls were aligned with the chamber model created in the software. Erlenmeyer flasks were put on top of the retainers to prevent subject mice from jumping on top of the retainers, a tracking free zone. This setup with open doors was used as background allowing motion tracking of the subject mouse. Prior to the start of the experiment illuminance of 93,4±1,8 lux was determined.

Day 1: Habituation
On the first day habituation (or training) was conducted in the setup shown in figure 9. One subject mouse after another was allowed to freely explore the empty arena (no object or stranger mouse present in the retainers) in a 10-minute period. After the trial the subject mouse was put in a separate cage to prevent influence on the mice that were not yet tested. Between trials the arena and retainers were cleaned with water and ethanol (50 v/v %). In a separate habituation trial, the stranger mice were allowed to sit in the retainers to get used to the environment.

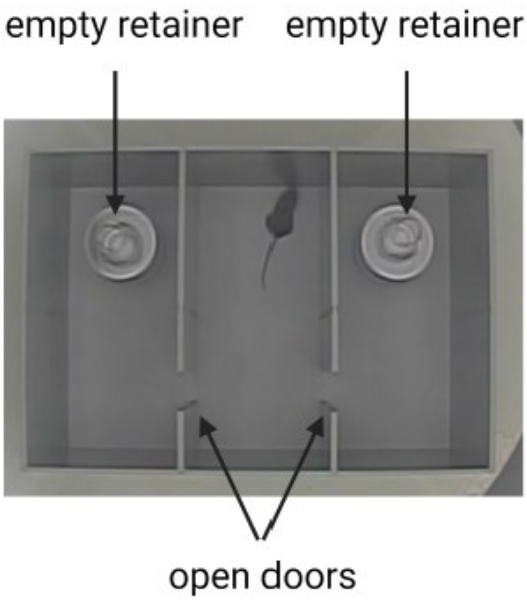

Figure 9 Habituation setup on day 1.
Subject mouse was placed in an empty arena with open doors for 10 minutes. The mouse was then allowed to freely explore the arena. Image was taken from tracking videos recorded by “Topscan” software.

Day 2: Social Interaction test

One day after habituation social interaction was conducted as shown in figure 10. A black novel object similar in size to a mouse was placed in one retainer and a stranger mouse matched in age and sex in the other. Location of the object and the unfamiliar mouse were alternated after each trial. The retainer, a wire cage, allowed olfactory, auditory, visual and some tactile interactions but not direct physical contact such as biting. Before the start of the recording the subject mouse was put in the middle chamber with closed doors. 5 seconds after pressing record in the program the doors were removed and the tracking started. The trial was conducted in a 5-minute period. Afterwards the subject mouse was put in a separate cage to prevent influence on the mice that were not yet tested. The stranger mouse was removed from the retainer and the arena cleaned with water and ethanol (50 v/v %) before the next trial.

The percentage of time spent in the chamber with the stranger, or the object was defined as a parameter for social interaction. The mouse was considered to be in the chamber when its head and four paws had entered into the chamber.

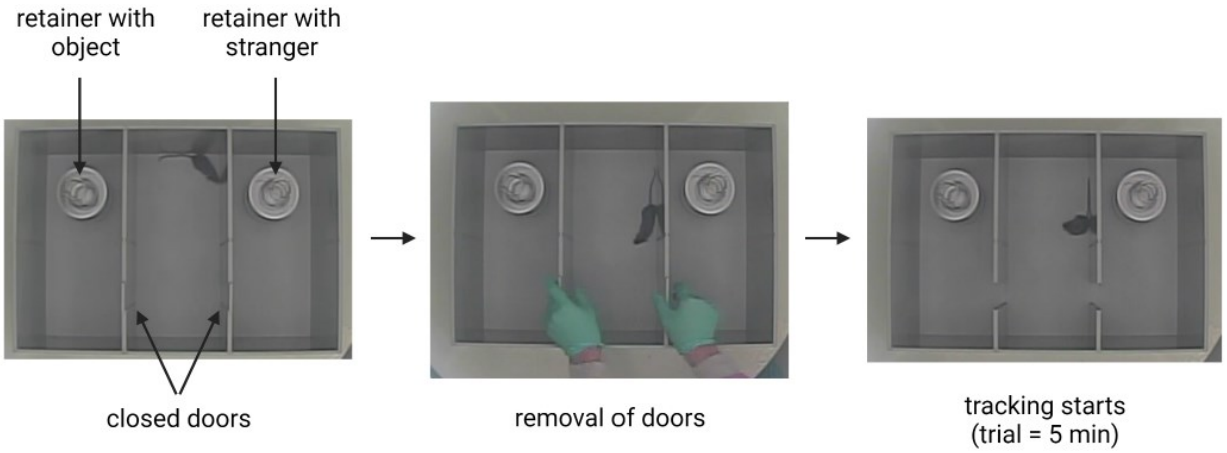

Figure 10 Steps conducted for the social interaction test.
Stranger mouse and object were put in the retainers first. Afterwards the subject mouse was placed in the middle chamber. Five seconds after pressing record in the "Topscan" program, doors were removed, and the tracking started. Trial lasted for 5 minutes. Images were taken from tracking videos recorded by the software "Topscan".

Social interaction data from the video tracking software "Topscan" (Cleversys, Inc.; USA) were exported and further analyzed using Microsoft® Excel® for Microsoft 365 MSO (Version 2302 Build 16.0.16130.20332) 64-bit. Data were sorted by sex and genotype and normalized. Percentage of time spent in the chamber with the stranger or object was defined as parameter for social interaction. Data from males and females were pooled as no sex difference was seen. Normalization was performed by dividing percentage of time spent in the chamber during the test with percentage of time spent in the chamber during the first 5 minutes of habituation. The reason for normalization was to show that a possible preference for a chamber during the test was due to the stranger mouse or the novel object and not due to a general preference of the subject mouse for the respective chamber seen on habituation. Prerequisite for inclusion of data were a correct trial setup including unfamiliar stranger mouse and novel object as well as that the subject mouse entered every chamber during habituation and test trial. For this reason, two mice were excluded from statistical calculations with the first being a *Gnpat* KO male, in which trial setup was not correct as the novel object in the other retainer was missing, and the second being a WT control male that did not enter the chamber with the stranger once during the 5-minute trial.

For the comparison of the preferences within each genotype, statistical analysis was performed using two-tailed Student's t-tests. For the comparison of the genotypes an index was calculated by subtracting normalized time spent in chamber with the stranger with normalized time spent in chamber with the object. Statistical analysis was then performed using ordinary one-way ANOVA with Tukey's correction for multiple comparisons.

2.1.7. Metabolic cage

Group-housed mice were given training drinking bottles with spill- and leak-protected nozzles provided by TSE Systems (Germany) twelve days prior the start of the experiment. Water was provided by pushing a pin in the middle of the nozzle, making exact measurement of water consumption of the subject mouse possible. One week prior to the experiment mice were single-housed and afterwards put individually in cages of the TSE PhenoMaster system (Germany, https://www.tse-systems.com/product-details/phenomaster) for 8 days with the same day-night rhythm (14:10 h) as before, a set temperature at 24±1°C and humidity of 50±10%. The open climate chamber of the TSE PhenoMaster system is shown in in figure 11. Locomotor activity was measured using ActiMot infrared sensor frames surrounding each cage, thus, allowing measurement of horizontal as well as vertical movement. Water and food consumption as well as the amount of CO_2 produced and O_2 consumed (with gas sampling values set at an airflow of 0.45 L/min) were measured every 15 minutes allowing calculation of respiratory exchange rate (RER) and energy consumption (indirect calorimetry, calculations based on (Weir, 1949)) with the provided TSE PhenoMaster software (Germany).
Wellbeing of the mice and setup parameters, such as temperature, humidity, and airflow were checked and documented daily. Water and food were refilled when necessary. Refilling was done while no measurement was performed in the respective box. One water bottle in a box with a WT control male was suspected to be leaking on day 2, when checking water consumption. Water bottle was changed during the check on day 3.

Raw data from the PhenoMaster were exported and further analyzed using Microsoft® Excel® for Microsoft 365 MSO (Version 2302 Build 16.0.16130.20332) 64-bit. Data were sorted by sex and genotype. Female data were not yet analyzed as the experiment was repeated with another female cohort. Only full days and nights were used for analysis. Sum of total ambulatory activity, defined as movement crossing more than one beam, and sum of total fine movement, defined as movement crossing only one beam, were calculated manually. For activity parameters (total horizontal movement, ambulatory movement, fine movement, vertical movement) and food and water consumption a sum for every full day (14 h) and full night (10 h) was calculated. Sums were then divided by number of hours to get the hourly activity or consumption for each day and night. Finally,

the average for all nights and all days was calculated and boxplots were drawn. Concerning water consumption, one water bottle was suspected of leaking on day 2 for one male WT. Bottle was changed on day 3 during the check. Drinking data of this box in this time period reinforced this assumption, thus, drinking data from day 2, night 3, day 3 for this box were excluded from analysis.

Parameters for metabolism such as oxygen consumption, carbon dioxide production, RER and for calorimetry were automatically set in relation to the body weights weighed before the start of the experiment. An average for every full day and full night was calculated. The average of all nights and all days was then calculated, and boxplots were drawn. Statistical analysis for all boxplots was performed by using ordinary one-way ANOVA with Tukey's correction for multiple testing. For better visualization line graphs with all measured data points were drawn, but not statistically analyzed.

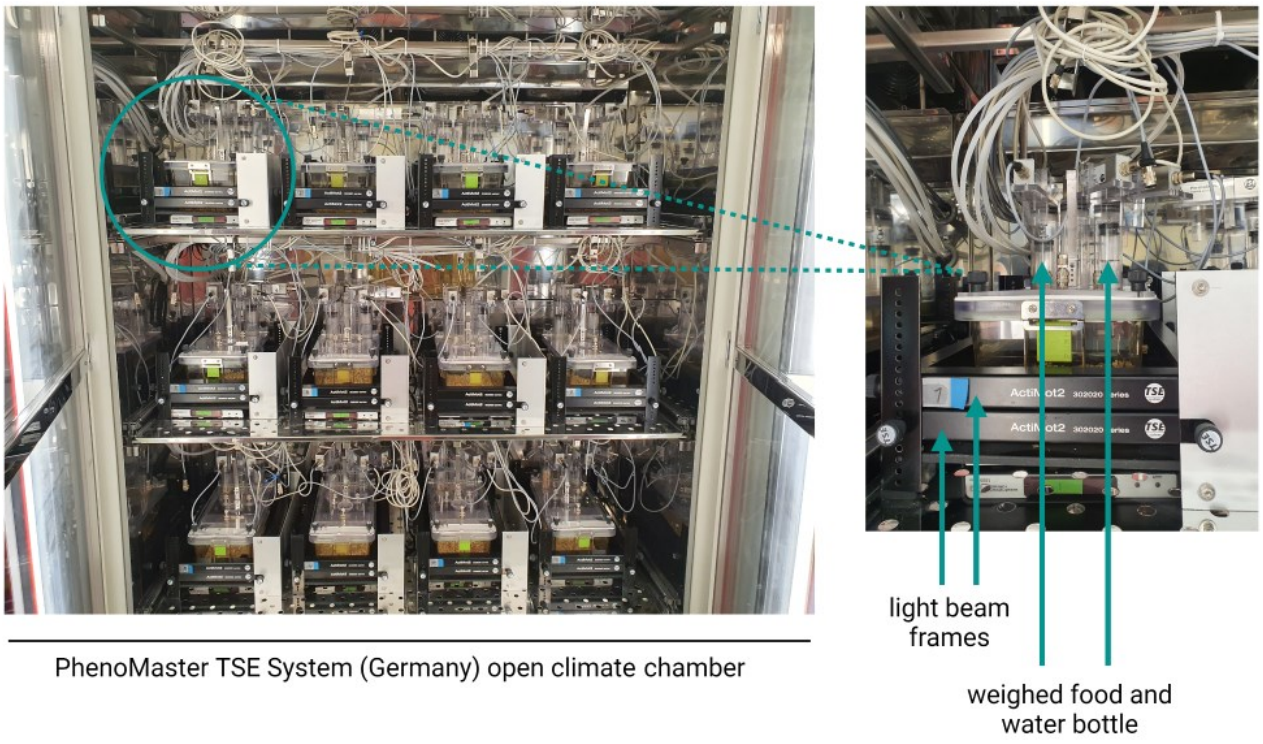

Figure 11 Open climate chamber of the PhenoMaster TSE System (Germany).
ActiMot light beam frames for measurement of locomotor activity and weighed food and water bottle for food and water consumption were highlighted. Images taken and used with permission from Sylvia Badurek and self-adapted.

2.1.8. Fear conditioning

Fear conditioning was performed using the Habitest modular system (Coulbourn Instruments, MA, USA, www.coulbourn.com) with the PT-600A 300W powerful amplifier system (Pyle, USA) both placed in a soundproof chamber using a previously published

protocol (Hagelkruys et al., 2022). For recording and quantification of freezing time the software FreezeFrame 3 (Actimetrics, IL, USA, www.actimetrics.com) was used.

Day 1: Training

Before the start of the experiment, tone was calibrated to 85±2 dB with the door of the soundproof chamber closed preventing mice from coming in contact with the sound prior the experiment. Operant cage was setup as shown in figure 12 with a lamp using house light in the visible range, a fan for ventilation, a connected grid for application of mild electric foot shock and grey tiles.

Training for association of a conditioned sound stimulus (CS = 85±2 dB, 10 kHz) to an aversive unconditioned electric foot shock stimulus (US = 0.5 mA, 2 s) was performed using the following protocol: Pre-phase (120 s, no shock or sound), first CS (30 s, sound) paired with an US in the last 2 s, inter-tone-interval (90 s, no shock or sound), second CS (30 s) paired with an US in the last 2 s, post-phase (70 s, no shock or sound). After the trial the subject mouse was put in separate cage to prevent contact with animals that were not yet tested. Operant cage was cleaned with water and ethanol (50 v/v %) between the trials.

Day 2: contextual fear conditioning

Contextual fear conditioning was conducted 24 h after training. The mice were put into the same environment using the operant cage setup from the day before. Subject animals were recorded for 4 min without sound or shock presentation and afterwards put in separate cages to prevent contact with animals that were not yet tested. Box was cleaned with water and ethanol (50 v/v %) between the trials.

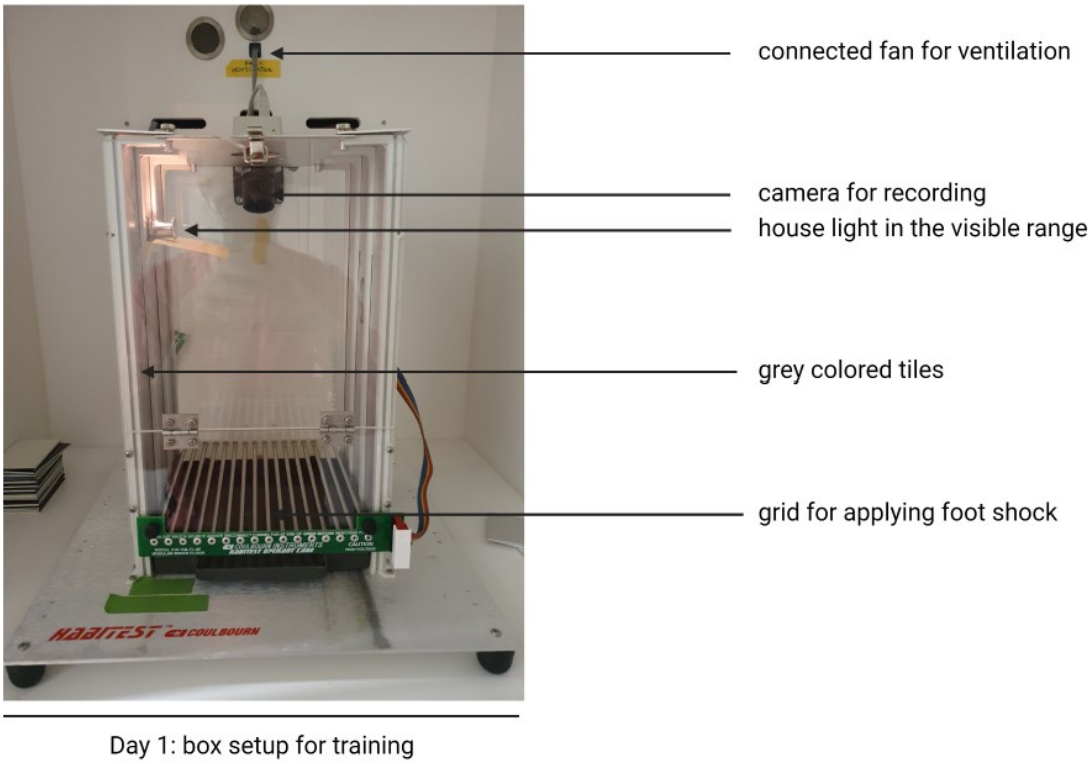

Figure 12 Operant cage setup on day 1 of fear conditioning.
Grid was connected for applying of mild electric foot shock as well as a fan for ventilation. Grey tiles and house light in the visible range was used. Image taken and used with permission from Sylvia Badurek and self-adapted.

Day 3: cued fear conditioning

On day 3 (48 hours after training) cued fear conditioning was performed. Prior to the start of the experiment, the tone was calibrated to 85±2 dB with the door of the soundproof chamber closed preventing mice from coming in contact with the sound prior to the experiment. Operant cage setup was changed as shown in figure 13. Fan was disconnected to prevent mice from reacting to the generated sound. Color of the tiles was changed to black and white. The lamp was switched to infrared house light. For different texture of the floor a plastic plate wrapped in paper towel was put on top of the grid. A different smell was created by placing a paper towel covered with a few drops of citrus oil beneath the floor.

Cued fear conditioning was performed using the following protocol: Pre-phase (120 s, no shock or sound), first CS (60 s, sound, no shock), inter-tone-interval (60 s, no shock or sound), second CS (60 s, sound, no shock), post-phase (60 s, no shock or sound). Afterwards mice were removed and put in separate cages from animals that were not yet tested.

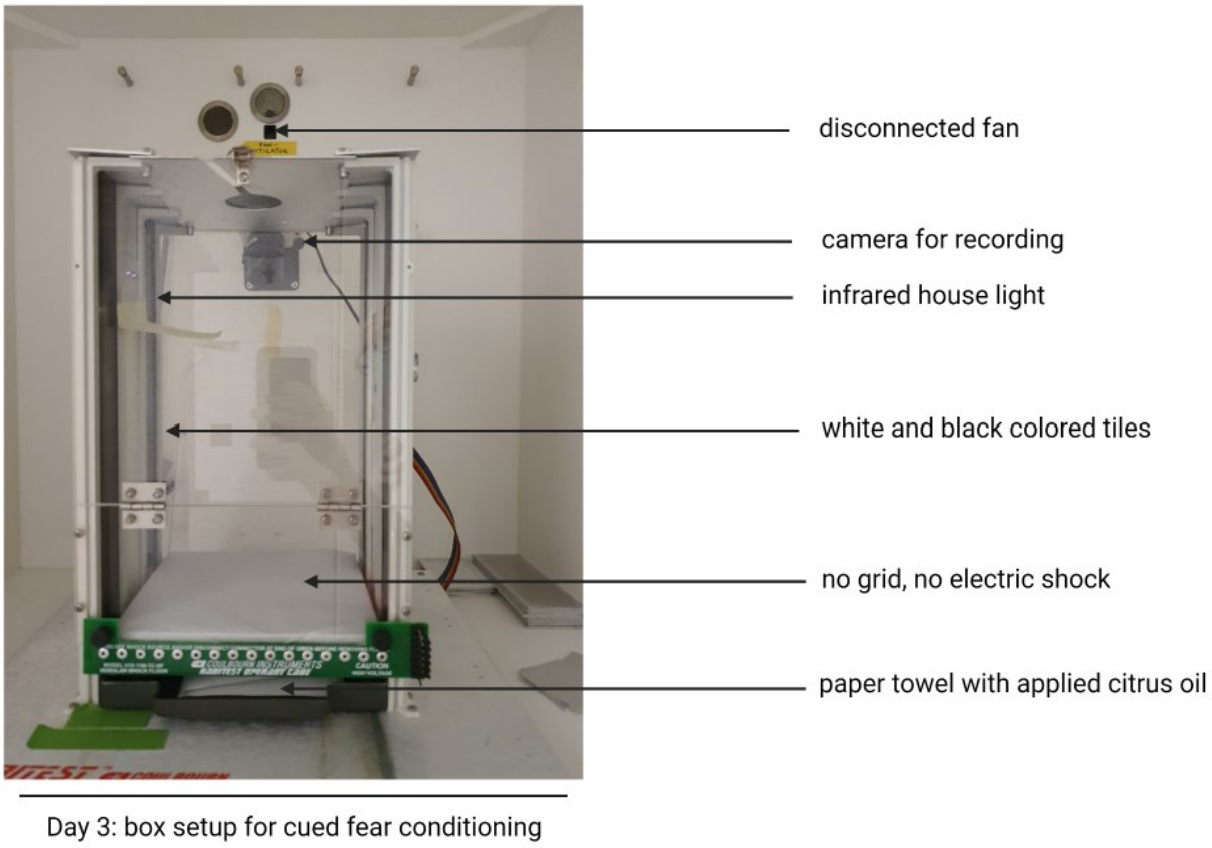

Figure 13 Operant cage setup for cued fear conditioning.
In comparison to the setup on day 1 and 2 the fan was disconnected, lamp was switched with a lamp using infrared house light, texture of the floor and color of the tiles was changed. Smell was adapted by applying a few drops of citrus oil on a paper towel and putting it beneath the floor. Image taken and used with permission from Sylvia Badurek and self-adapted.

For quantification of freezing time, all recorded videos were analyzed with the software FreezeFrame 3 (Actimetrics, IL, USA, www.actimetrics.com). Freezing was defined as a lack of motion for at least 2 s except for breathing motion. Suggested freezing by the software was then manually checked to see if freezing was identified correctly. It was adjusted if needed by setting a different threshold. Data were then exported and further analyzed using Microsoft® Excel® for Microsoft 365 MSO (Version 2302 Build 16.0.16130.20332) 64-bit. Data were sorted by sex and genotype. Data from males and females were pooled as no sex difference was observed.

Ordinary one-way ANOVA with Tukey's correction for multiple comparisons was used for statistical analysis of contextual fear conditioning. Statistical analysis for cued fear conditioning was performed using ordinary one-way ANOVA for every time point (Pre-CS, first CS, inter-tone-interval, second CS, post-CS) with Bonferroni correction for multiple testing by multiplying p-value of the ANOVA with 5 for the 5 different time points. If p-values were still significant ($p < 0.05$), Tukey's tests for pairwise comparisons of the genotypes were performed, if not pairwise comparisons were also determined as not significant.

3.1. Social Interaction

A behavioral phenotype mimicking aspects of human psychiatric disorders was found in experiments with *Gnpat* KO males (Dorninger et al., 2019a). As mentioned in section 1.2.4 preference for the stranger mouse was reduced in *Gnpat* KO males compared to their WT controls. It was hypothesized that the presence of non-vinyl ether phospholipids alleviates impaired social interaction. Therefore, to assess the influence of vinyl ether and non-vinyl ether phospholipids on social interaction the experiment was repeated by using *Gnpat* KO, *Peds1* KO and WT mice as control group.

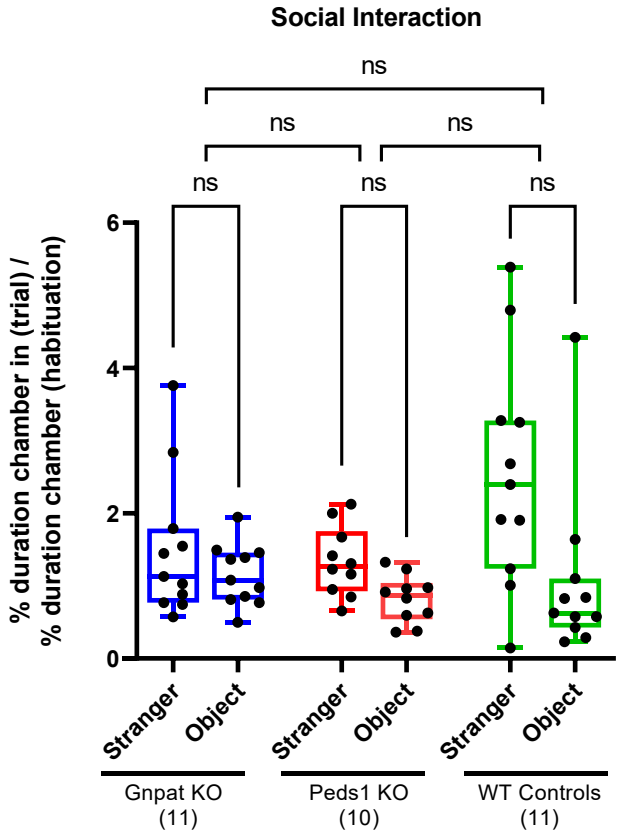

Figure 14 Social interaction test of *Gnpat* KO, *Peds1* KO and WT controls.
No significant differences were seen in comparison between the groups as well as in the comparison within each group. Percentage of time spent in the whole chamber with the stranger, or the object was used for social interaction and was quantified automatically. Data were normalized by dividing percentage of time spent in the respective chamber on the day of the test with percentage of time spent in the chamber with the stranger or object during the first 5 minutes of habituation. Data are shown as box plots with individual data points, with whiskers indicating lowest and highest values. For comparison of the preferences within each genotype two-tailed Student's t-tests were used for statistical analysis. For comparison between the genotypes an index using the difference between normalized time spent in chamber with the stranger and normalized time spent in chamber with the object was calculated. Statistical analysis was then performed by using ordinary one-way ANOVA. n.s., not significant.

The percentage of time spent in the chamber with an unfamiliar stranger mouse (matched in age and sex) as well as the percentage of time spent in the chamber with a novel object

were measured, quantified, and normalized for evaluation of social interaction. According to the two-tailed Student's t-tests the experiment revealed no significant preference for the chamber with the stranger or the chamber with the novel object in all groups (*Gnpat* KO P = 0.3905; *Peds1* KO P = 0.0641; WT Controls P = 0.0796). In addition, no significant difference between the groups was observed when using ordinary one-way ANOVA with Tukey's multiple comparisons test.

3.2. Metabolic cage

3.2.1. Locomotor activity

In different settings hyperactivity was shown in *Gnpat* KO mice (Dorninger et al., 2019b). However, the involving experiments never lasted longer than 61 minutes. In order to determine if this effect is also displayed in a long-term setting, *Gnpat* KO mice were put in individual metabolic cages for 8 days. In *Peds1* KO mice, no behavioral experiments, including experiments measuring locomotor activity, were performed. *Peds1* KO in comparison to *Gnpat* KO mice were used to investigate the effects of vinyl ether and non-vinyl ether phospholipids on locomotor activity, with wildtype animals acting as control group.

In general, all mice were more active at night than during the day, as shown in figure 15 (C). A shift between day and night was shown in all measured parameters, thus, diurnal and nocturnal data were analyzed separately. The total horizontal activity was defined as the sum of ambulatory movement and fine movement. In line with previous experiments, *Gnpat* KO males showed significantly higher activity at night as well as during the day compared to their WT controls. This behavior did not diminish over time but was visible throughout the experiment as seen in figure 15 (C). The *Peds1* KO males also showed significantly higher nocturnal activity than their WT controls, but no significant difference in diurnal activity compared to their WT controls. In addition, no significant difference in nocturnal and diurnal activity was seen between *Gnpat* KO and *Peds1* KO males.

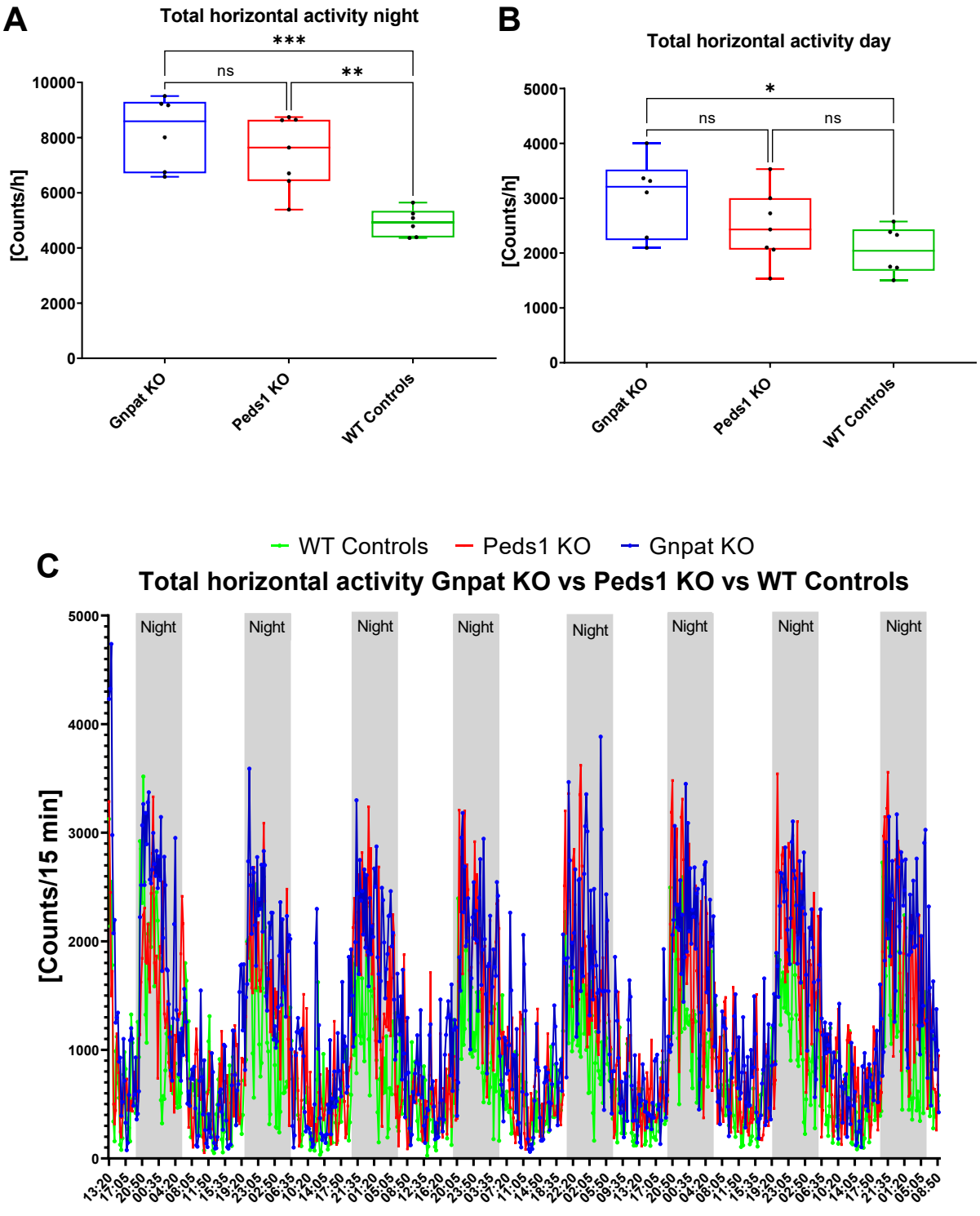

Figure 15 Total horizontal activity of *Gnpat* KO, *Peds1* KO and WT controls.
Gnpat KO males (n=6), *Peds1* KO males (n=7), WT control males (n=6) were put in metabolic cages for 8 days. Movement counts were measured with light beams about 1 cm apart. (A) and (B) show average movement at night or day calculated as counts/h. Only full days were used for calculations and statistical analysis. Data are shown as box plots drawn with individual data points, with whiskers indicating highest and lowest values. Statistical analysis was performed using ordinary one-way ANOVA with Tukey's multiple correction tests for pairwise comparison between each group. (C) Line graph was drawn for better visualization of the variability during the day and night. No statistical analysis was performed. All 15 minute-intervals were plotted against measured counts. Grey blocks were manually drawn and indicate night period. The artificial day lasted from 6 am to 8 pm and the night from 8 pm to 6 am. *** P < 0.001; ** P < 0.01; * P < 0.05; n.s., not significant.

Ambulatory activity defined as forward moving motion involving the consecutive interruption of different light beams in the horizontal plane was again generally higher at night than during the day (König et al., 2020). The results for ambulatory activity from figure 17 (A and B) showed the same trends as the results from figure 15. *Gnpat* KO males were displaying significantly higher nocturnal and diurnal ambulatory activity compared to their WT controls. Nocturnal ambulatory movement in *Peds1* KO males was also significantly increased. However, no significant difference in diurnal ambulatory activity was measured. Additionally, as seen in total horizontal activity, no difference in nocturnal and diurnal ambulatory activity was shown between *Gnpat* KO and *Peds1* KO males.

Figure 17 (C and D) shows the results for fine activity. Fine activity was reflecting the same trends as in ambulatory activity with *Gnpat* KO and *Peds1* KO males displaying significantly higher nocturnal fine activity than WT controls, whereas during the day no significant differences in fine activity were seen. Fine activity was defined as stationary movement repeatedly breaking the same light beam such as grooming (König et al., 2020).

Figure 17 (E and F) shows average nocturnal and diurnal vertical activity of *Gnpat* KO, *Peds1* KO and WT control males. Vertical activity or rearing was defined as all movement breaking beams in the z plane (König et al., 2020). In line with ambulatory and fine activity, *Gnpat* KO and *Peds1* KO males showed significantly higher vertical activity than WT controls at night, but not during the day.

In addition, we have also independently analyzed the data from habituation of the three-chamber trial, in which the subject mice could freely explore the empty arena for 10 minutes. The distance covered by the subject mice was determined and used as experiment on exploratory behavior in an enriched environment. Figure 17 shows *Gnpat* KO and *Peds1* KO mice ran significantly farther than their WT controls.

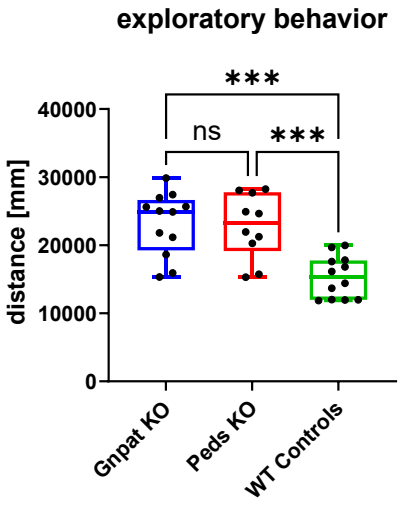

Figure 16 Exploratory behavior in an enriched environment of *Gnpat* KO, *Peds1* KO and WT controls
Gnpat KO (n=12), *Peds1* KO (n=10) and WT controls (n=12) were individually put in the empty three-chamber arena for habituation on day prior the start of the social interaction experiment. The subject mice were allowed to freely explore the enriched environment for 10 minutes. Distance traveled was automatically calculated. Data are shown as box plots drawn with individual data points, with whiskers indicating highest and lowest values. Statistical analysis was performed using ordinary one-way ANOVA with Tukey's multiple correction tests for pairwise comparison between each group. *** $P < 0.001$; n.s., not significant.

In summary, our findings support previous experiments with *Gnpat* KO males showing overall higher activity in *Gnpat* KO males than in WT controls throughout the entire period of the experiment. In addition, the results indicate a hyperactive phenotype also in *Peds1* KO males.

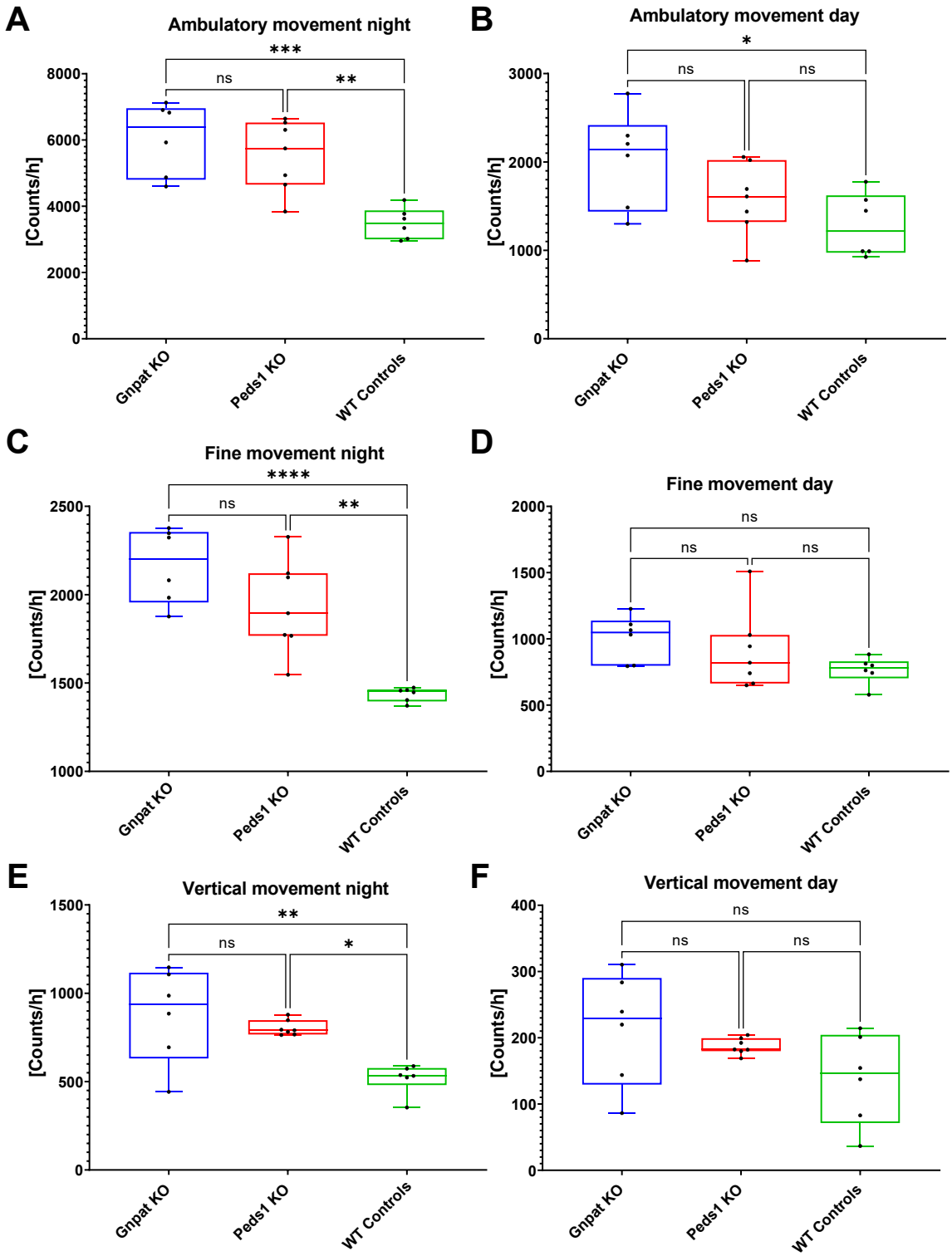

Figure 17 Ambulatory, fine and vertical movement of *Gnpat* KO, *Peds1* KO and WT controls.
Ambulatory, fine and vertical movement of *Gnpat* KO males (n=6), *Peds1* KO males (n=7) and WT controls (n=6) were measured for 8 days using light beams about 1 cm apart as well as light beams in the z plane. Ambulatory movement is defined as forward moving motion crossing more than one light beam. Fine movement is defined as the breaking of only one light beam. Vertical movement included all movement breaking beams in the z plane. (A), (B), (C), (D), (E), (F) show average movement at night or day calculated as counts/h. Only full days and full nights were used for calculations and statistical analysis. The artificial day lasted from 6 am to 8 pm and the night from 8 pm to 6 am. Box plots are drawn with individual data points, with whiskers indicating highest and lowest values. Statistical analysis was performed using ordinary one-way ANOVA with Tukey's multiple correction tests for pairwise comparison between each group. **** $P < 0.0001$; *** $P < 0.001$; ** $P < 0.01$; * $P < 0.05$; n.s., not significant.

3.2.2. Metabolism

In order to get insights into possible changes in metabolism in *Gnpat* KO and *Peds1* KO mice due to changes in ether phospholipids measurements of oxygen consumption, carbon dioxide production were taken, and respiratory exchange ratio (RER) and energy consumption were calculated. In addition, measurements of food and water consumption were evaluated.

Oxygen consumption and carbon dioxide production need to be examined in the broader context of respiratory exchange ratio and energy expenditure. The former represents the ratio of expired carbon dioxide divided by oxygen taken up by the lungs. RER changes to a variety of factors such as level of activity, type of food, day or night time, temperature, strain and in some cases sex (Bi et al., 2014; Colon-Mesa et al., 2023; Even and Nadkarni, 2012; König et al., 2020; Marvyn et al., 2016). In general, a RER of 1.0 indicates carbohydrates as primary source of fuel as in the oxidation of carbohydrates the ratio of required oxygen molecules to carbon dioxide molecules produced is 1:1. Combustion of fatty acids requires more oxygen than for carbohydrates leading to a lower ratio of 0.7 (Even and Nadkarni, 2012; König et al., 2020). Standard feed as used in our experiment, consists mainly of carbohydrates and typically results in nocturnal RER values between 1.0 to 0.7, but closer to 1.0. During the light phase, when mice are more inactive, RER decreases indicating a shift to combustion of endogenous lipids to sustain metabolism (König et al., 2020; Marvyn et al., 2016). In our study, the general O_2 consumption and CO_2 production were higher at night than during the day, when mice were less active. As shown in figure 18, both oxygen consumption as well as carbon dioxide production were significantly higher in *Gnpat* KO males during the night compared to WT controls, possibly affected by the higher locomotor activity of *Gnpat* KO mice. Interestingly, higher activity in *Peds1* KO males did not lead to significantly higher O_2 consumption and CO_2 production at night when compared to WT controls. However, a trend was visible with *Peds1* KO males seeming to lie between WT controls and *Gnpat* KO mice. No differences were seen in O_2 consumption and CO_2 production during the day in all groups.

RER as shown in figure 19 (C) revealed the same variations between day and night that is possibly caused by a shift in fatty acid combustion as well as lower activity. In addition, an adjustment period to the metabolic cage was visible, especially in *Gnpat* KO mice. Levels of nocturnal RER were in line with RER values in relation to standard chow as feed suggesting carbohydrates as primary source of fuel. Although no significant differences in nocturnal RER could be seen between the groups two points are interesting

when looking at diurnal RER as shown in figure 19 (B). Firstly, diurnal RER values were lower than nocturnal RER values confirming a general shift to fatty acid combustion during the day. Secondly, diurnal RER was significantly lower in *Gnpat* KO and *Peds1* KO males compared to WT animals.

Energy expenditure is divided into basal metabolic rate, which is measured in a thermoneutral environment (29-31°C) in fasted and resting animals, thermoregulation, thermic effect of feeding (nutrient digestion) and the energy consumption of activity (Even and Blais, 2016). In addition, body mass, body composition, strain and sex can influence energy expenditure (König et al., 2020). As shown in figure 18 (E and F) *Gnpat* KO males displayed significantly higher energy expenditure than WT controls, possibly due to the general higher activity in *Gnpat* KO mice. Interestingly, no differences in diurnal energy expenditure could be observed, even though *Gnpat* KO males displayed significantly higher activity and weighed significantly less (figure 20 (E)) than WT controls. Nocturnal and diurnal energy expenditure in *Peds1* KO was not significantly different compared to both *Gnpat* KO and WT control animals, even though, they also displayed higher activity at night compared to their WT controls suggesting attenuated energy consumption.

Growth deficits were previously described for *Gnpat* KO mice (Rodemer et al., 2003). Accordingly, body weight was significantly lower in *Gnpat* KO males than in WT controls and in *Peds1* KO mice as shown in figure 20 (E). No significant differences in body weight were measured between *Peds1* KO males and WT controls. Considering that the *Gnpat* KO mice were smaller but more active and therefore expended more energy than WT controls, it must be highlighted that no significant difference in food and water consumption was found. However, food consumption in WT controls was significantly higher at night compared to *Peds1* KO mice, even though no differences in bodyweight were determined and greater activity was observed in *Peds1* KO males at night.

To conclude, our data indicate metabolic changes affecting growth, O_2 consumption, CO_2 production and energy expenditure in *Gnpat* KO mice. In *Peds1* KO mice, the metabolic changes appear to be attenuated or overall absent.

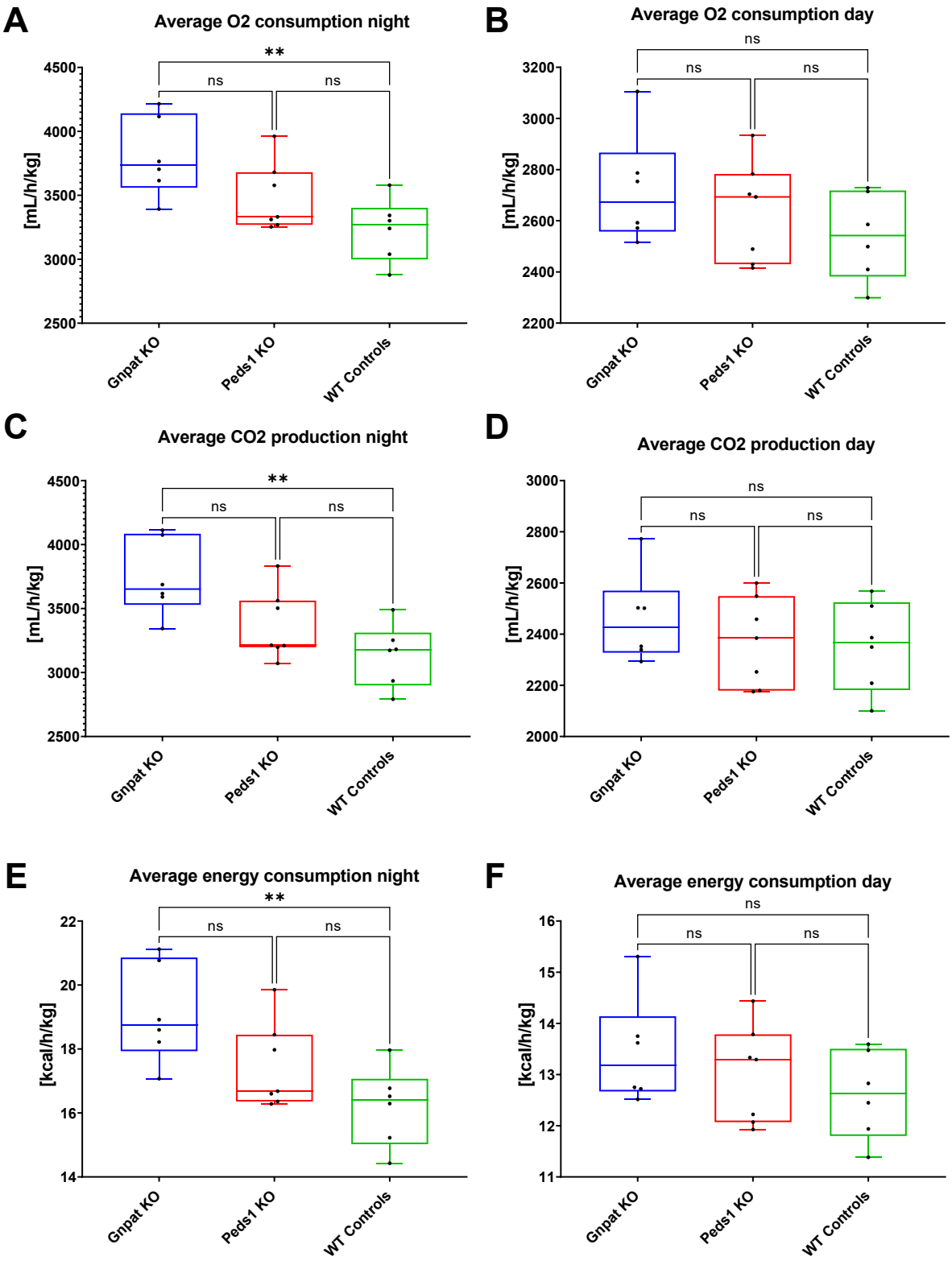

Figure 18 O_2 consumption, CO_2 production and energy consumption of *Gnpat* KO, *Peds1* KO and WT control males.

O_2 consumption and CO_2 production of *Gnpat* KO males (n=6), *Peds1* KO males (n=7) and WT controls (n=6) were measured by gas sampling every 15 minutes. Energy consumption (indirect calorimetry) was calculated automatically using measurements of O_2 consumption and CO_2 production. Calculations are based on (Weir, 1949). (A), (B), (C), (D), (E), (F) show averaged values of all full nights or full days. The artificial day lasted from 6 am to 8 pm and the night from 8 pm to 6 am. Box plots are drawn with individual data points, with whiskers indicating highest and lowest values. Statistical analysis was performed using ordinary one-way ANOVA with Tukey's correction for multiple testing. ** $P < 0.01$; * $P < 0.05$; n.s., not significant.

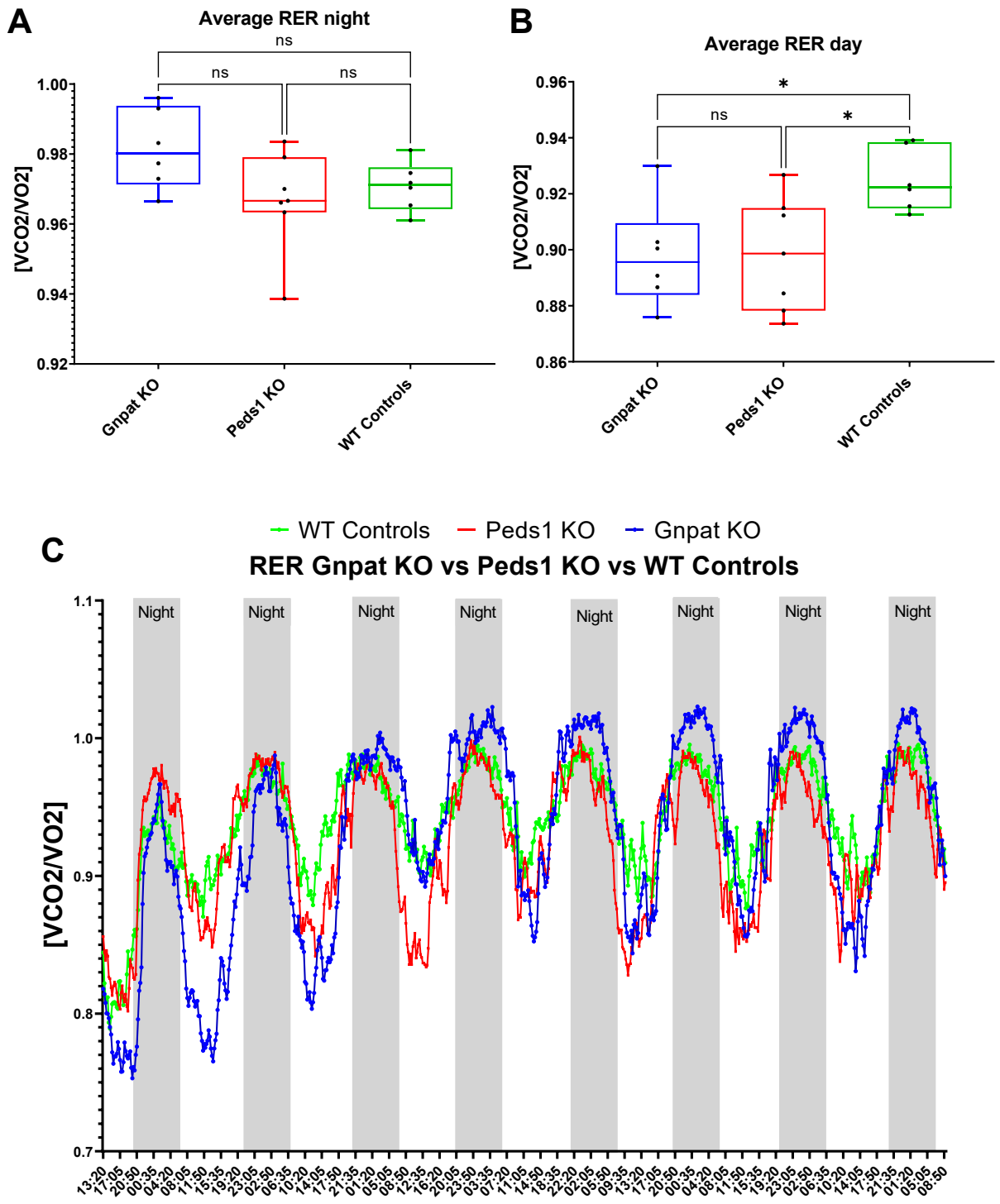

Figure 19 Respiratory exchange ratio of *Gnpat* KO, *Peds1* KO and WT controls.
Respiratory exchange ratio (RER) was calculated from measurements of O_2 consumption and CO_2 production of *Gnpat* KO males (n=6), *Peds1* KO males (n=7) and WT controls (n=6). (A) and (B) show average RER at night or day. Only full days were used for calculations and statistical analysis. Box plots are drawn with individual data points, with whiskers indicating highest and lowest values. Statistical analysis was performed using ordinary one-way ANOVA with Tukey's multiple correction tests. (C) Line graph was drawn for better visualization of the variability during the day and night as well as to visualize the adjustment period in the beginning. No statistical analysis was performed. All 15 minute-intervals were plotted against measured counts. Grey blocks were manually drawn and indicate night period. The artificial day lasted from 6 am to 8 pm and the night from 8 pm to 6 am. * $P < 0.05$; n.s., not significant.

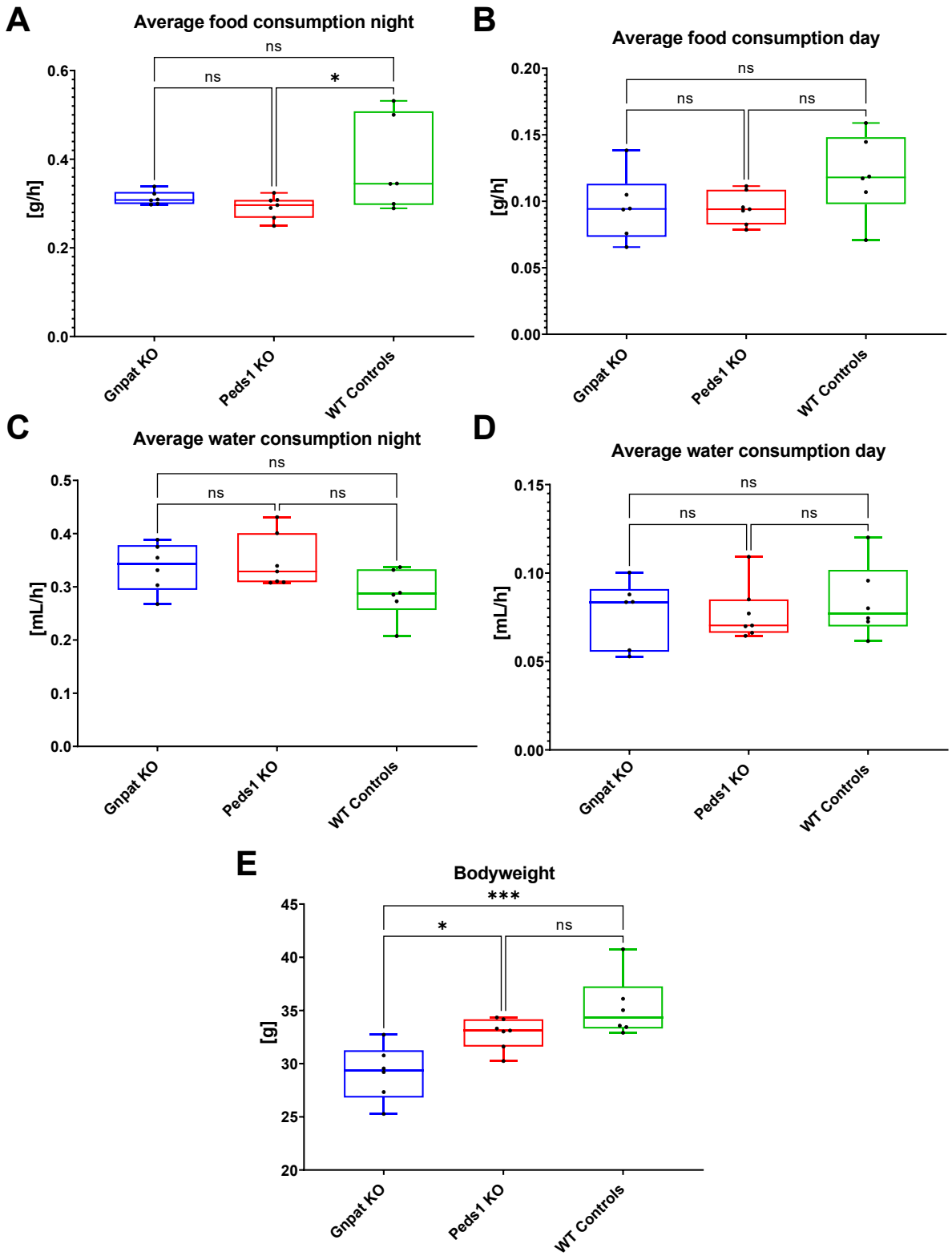

Figure 20 Food and water consumption of *Gnpat* KO, *Peds1* KO and WT controls as well as bodyweight before the start of the metabolic cage.
Food and water consumption for 8 days was determined by precise weighing sensors measuring the amount of food and liquid consumed from the hanging water and food bottle. Bodyweight was measured before putting mice in the metabolic cage. (A), (B), (C), (D) show average food and water consumption at night or day calculated as g/h or mL/h. The artificial day lasted from 6 am to 8 pm and the night from 8 pm to 6 am. Box plots are drawn with individual data points, with whiskers indicating highest and lowest values. Only full days or full nights were used for statistical analysis. Statistical analysis was performed using ordinary one-way ANOVA with Tukey's correction for multiple testing. *** $P < 0.001$; * $P < 0.05$; n.s., not significant.

3.3. Fear conditioning

In previous experiments, it was shown that *Gnpat* KO males displayed reduced contextual and cued fear conditioning. In order to elucidate the role of vinyl ether and non-vinyl ether phospholipids on fear conditioning the experiment was performed again using *Gnpat* KO mice, *Peds1* KO mice and WT mice as controls.

Figure 20 (A) shows freezing time of *Gnpat* KO, *Peds1* KO and WT control mice during the 4-minute contextual fear trial performed 24 hours after training session, in which mice react to the same environment used in training but not to a tone or shock. Previous results concerning *Gnpat* KO mice showed reduced freezing response (Dorninger et al., 2019a). In our experiment, *Gnpat* KO mice also displayed significantly reduced freezing time compared to WT controls. Worth mentioning is that *Peds1* KO mice also showed significantly reduced freezing response compared to WT controls with no significant difference between *Gnpat* KO and *Peds1* KO mice suggesting a more prominent role of plasmalogens in contextual fear conditioning.

Figure 20 (B) shows freezing response of *Gnpat* KO, *Peds1* KO and WT control mice during the different phases of the cued fear conditioning trial. Low freezing response during the pre-phase, in which no tone is presented, indicates that the setup of the operant cage was changed enough for the mice not to recognize the environment. Previous findings on *Gnpat* KO mice displaying reduced freezing response when presented with a tone were shown again. *Gnpat* KO mice spent significantly less time freezing when presented with a tone (1. CS and 2. CS) compared to WT controls. *Peds1* KO mice also showed significantly reduced freezing response when presented with a conditioned stimulus compared to WT controls. However, no significant difference in freezing time was seen between *Gnpat* KO and *Peds1* KO mice during the presentation of the first conditioned stimulus, whereas in comparison, *Peds1* KO mice showed significantly higher freezing response during the presentation of the second conditioned stimulus compared to *Gnpat* KO mice.

In summary, both *Gnpat* KO and *Peds1* KO mice displayed significantly reduced freezing response in fear conditioning suggesting evident memory deficits.

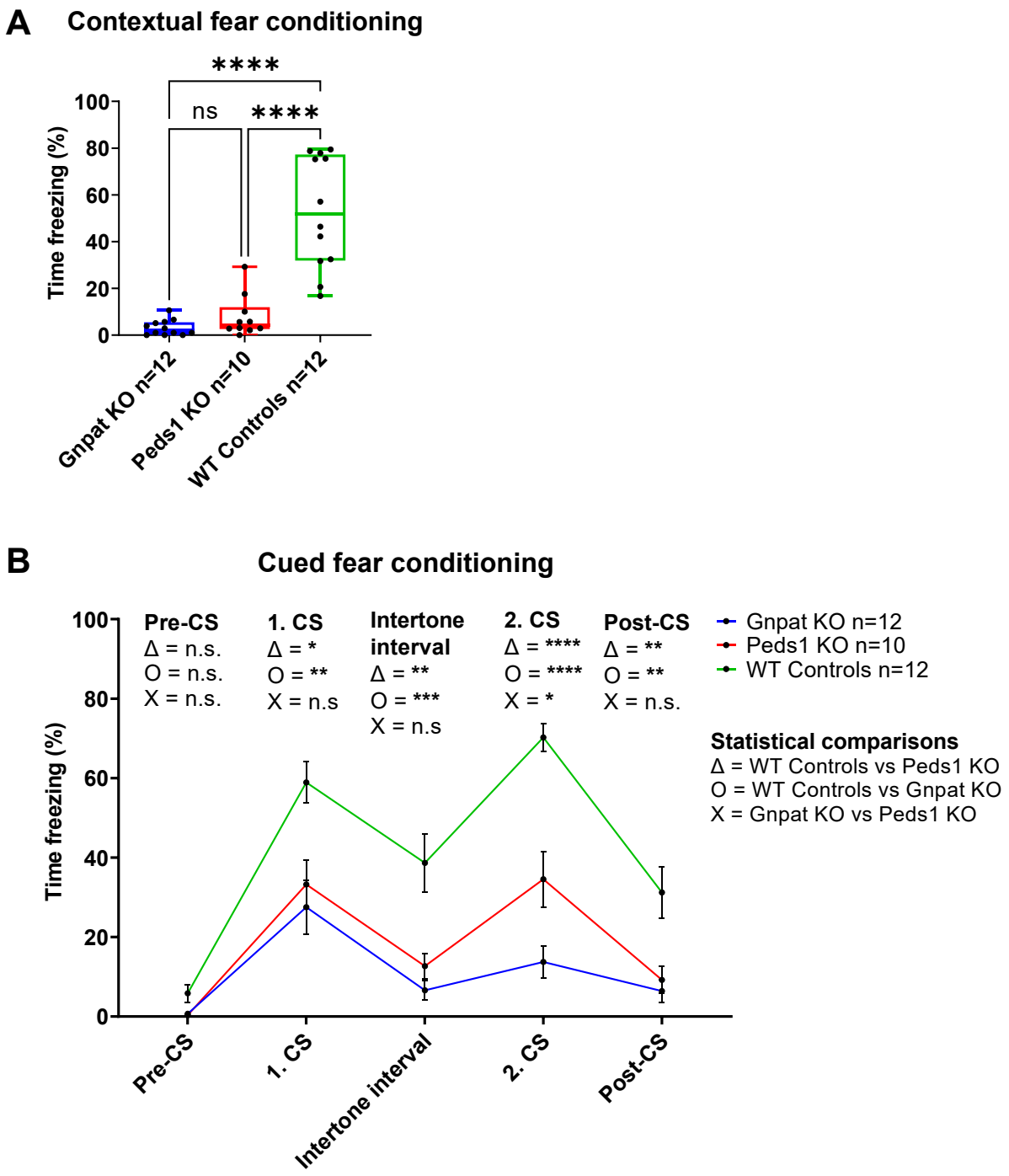

Figure 21 Contextual and cued fear conditioning of *Gnpat* KO, *Peds1* KO and WT control mice
Gnpat KO mice and *Peds1* KO showed impaired fear conditioning: (A) Contextual fear conditioning was applied to *Gnpat* KO mice, *Peds1* KO and WT controls 24 h after training by placing the mice into the operant cage with the same setup as used in training for 4 minutes without tone or shock presentation. Percentage of freezing time is shown as box plot, with whiskers indicating highest and lowest values. Statistical analysis was performed using ordinary one-way ANOVA with Tukey's correction for multiple testing. (B) Cued fear conditioning was performed 24 h after contextual fear conditioning using a changed operant cage setup. Freezing response was quantified for the different phases of the trial (Pre-CS, 1.CS, intertone interval, 2.CS, post-CS). Data are shown as mean ± SEM. Statistical analysis was performed using ordinary one-way ANOVA for every phase of the trial with Bonferroni correction for multiple testing. If p-values were still significant ($p < 0.05$) Tukey's tests for pairwise comparisons of the genotypes were performed, if not pairwise comparisons were also determined not significant. **** $P < 0.0001$; *** $P < 0.001$; ** $P < 0.01$; * $P < 0.05$; n.s., not significant

4 DISCUSSION

This study investigated how the presence or absence of non-vinyl and vinyl ether phospholipids affected mouse behavior, complementing previous studies revealing a disturbed behavioral phenotype with reduced social interaction, hyperactivity and impaired fear conditioning among other impaired behavioral aspects (Dorninger et al., 2019a, 2019b). It was hypothesized that the presence of non-vinyl ether phospholipids in *Peds1* KO mice alleviates the impaired behavior. In this study, we extend previous findings concerning hyperactivity, compromised social interaction and impaired fear conditioning in *Gnpat* KO mice. Additionally, we strengthen our hypothesis that impaired behavioral traits were attenuated in *Peds1* KO mice.

Social interaction in *Gnpat* KO, *Peds1* KO and WT controls was first assessed, using percentage of time spent in the chamber with the stranger or the chamber with the novel object as parameter for social interaction. In our experiment neither a significant preference for one chamber within the groups, even in the WT controls, nor a significant difference between the groups was revealed. However, a trend similar to previous findings from Dorninger et al. (2019a) showing a higher preference for the stranger in WT animals than in *Gnpat* KO was visible. According to this trend, the *Peds1* KO mice appeared to be between *Gnpat* KO and WT control mice, which strengthens our hypothesis that non-vinyl ether phospholipids alleviate impaired social interaction.
Differences in experimental setup need to be mentioned, when comparing our findings to the previous experiments from Dorninger et al. (2019a). First, in our experiments not only male *Gnpat* KO mice and WT controls were used. Secondly, while Dorninger et al. (2019a) applied a protocol of 30 minutes of habituation and 10 minutes for the sociability test, in our experiment habituation lasted 10 minutes and the sociability test 5 minutes, respectively. In addition, a different parameter was used for social interaction. Dorninger et al. (2019a) defined percentage of time spent with interaction partner as the percentage of time the subject mouse spent in direct contact with the stranger or the object. Lastly, Dorninger et al. (2019a) did not normalize their data. In literature, both time spent in the chamber as well as time spent sniffing (or in direct contact with the stranger or object) are commonly used as parameters to measure social interaction, either alone or in combination with other parameters such as the number of entries into the side chamber (Atanasova et al., 2023; Crawley, 2023; Kaidanovich-Beilin et al., 2011; Kashii et al.,

2023; Kurihara et al., 2023; Nadler et al., 2004; Nakamoto et al., 2020; Pignataro et al., 2023; Rapanelli et al., 2023; Rienecker et al., 2023; Shiwaku et al., 2023; Wang et al., 2023; Yang et al., 2011). The reason for using % time spent in chamber as parameter for social interaction in our experiment can be explained as followed: We argued that the subject mouse presumably knew that another mouse is in the side chamber when placing it into the center chamber due to their distinct sense of smell. The subject mouse then actively chose to either go into the chamber with the unfamiliar mouse or to the chamber with the object and spent time in there. According to our interpretation, this action can be considered as social interaction. However, Crawley et al. (2023) recommended measuring the time spent in direct contact with the unfamiliar mouse or the new object (usually a 2 cm sniffing zone around the retainer) like Dorninger et al. (2019a) used in their experiments with *Gnpat* KO males, as it was from their point of view a more accurate measure of social interaction, because the subject mouse can also choose to spend time sitting in a corner, rather than approaching the unfamiliar mouse. Besides using time spent in the sniffing zone as parameter, Crawley et al. (2023) also recommended to use time spent in the center chamber as well as total entries into the side chambers to identify general exploratory locomotion for a more sophisticated analysis.
Considering our findings, a foundation for further investigations into the role of vinyl ether and non-vinyl ether phospholipids on social interaction was laid. However, further experiments could be performed to confirm the observed trend. An extension of the sociability test to 10 min could be considered as studies showed that the majority of social approach is captured in the first 10 minutes (Crawley, 2023). This suggestion is in line with observations in our experiment, in which one male wildtype mouse did not go into the chamber with the stranger during the five-minute sociability trial but entered the chamber after the tracking and video stopped recording. Further experiments with a new cohort of mice performing reciprocal social interaction, a behavioral assay for direct social interaction in freely moving mice, could additionally strengthen our findings (Crawley, 2023).

For the first time locomotor activity over a time period of 8 days and metabolic parameters were assessed in *Gnpat* KO and *Peds1* KO mice. Locomotion is influenced by a number of factors, such as exploratory behavior, anxiety, novelty seeking, general health but also gender, strain and many more (König et al., 2020). While we can assume that exploratory behavior and possibly novelty seeking, a behavior to experience novel events and stimuli,

diminishes over time, nocturnal ambulator and fine activity in both *Gnpat* KO and *Peds1* KO males as well as diurnal ambulatory and fine activity in *Gnpat* KO males stayed significantly higher than WT controls throughout the entire experiment, thus, repeating the same trends already seen in the open field test performed by Dorninger et al. (2019b) using *Gnpat* KO and WT control males. Interestingly, nocturnal rearing (or vertical activity) considered as exploratory behavior was also increased in both *Gnpat* KO and *Peds1* KO compared to WT animals. In addition, our experiment on exploratory behavior in an enriched environment during habituation in the three-chamber arena revealed *Gnpat* KO and *Peds1* KO mice ran significantly farther than their WT controls. Our findings substantiate previous observations of hyperactivity in *Gnpat* KO males (Dorninger et al., 2019b). In addition, increased activity in *Peds1* KO males suggests the presence of an attenuated but still hyperactive phenotype and thus, a more prominent role of plasmalogens in hyperactivity.

Besides locomotion, our findings also allowed insight into the metabolism of *Gnpat* KO and *Peds1* KO males. While observations on reduced body weights in *Gnpat* KO mice confirmed already known phenotypic traits described by Rodemer et al. (2003), other parameters such as energy expenditure and food and water consumption as well as respiratory exchange ratio were investigated for the first time in *Gnpat* KO and *Peds1* KO mice. Respiratory exchange ratio, carbon dioxide production and oxygen consumption are interesting in the context of mitochondrial respiration efficiency. Inefficiency in mitochondrial respiration or increased mitochondrial uncoupling is linked to higher oxygen consumption and therefore results in lower RER values (Boudina et al., 2005; Park et al., 2019; Salin et al., 2019). This could explain the increased shift to a significantly lower diurnal RER in *Gnpat* KO males compared to WT animals. During the night this shift was possibly masked by higher activity in *Gnpat* KO males. In *Peds1* KO males this increased shift to lower diurnal RER was also shown suggesting that plasmalogens are important for mitochondrial respiration. Interestingly, it was found that ether phospholipids, especially plasmalogens, play an important role in mitochondrial homeostasis (Chen et al., 2023; Wanders et al., 2023). A deficiency in plasmalogens could lead to decreased expression of components of the respiratory chain encoded by mitochondrial DNA and thus, to disturbances in mitochondrial respiration (Wanders et al., 2023). Interestingly, positive links between mitochondrial efficiency and growth rate were found in a number of studies (Salin et al., 2019).

The increased nocturnal energy expenditure in *Gnpat* KO males was possibly caused by the increased activity. To get clearer insight into the energy metabolism of *Gnpat* KO and *Peds1* KO mice, a new experiment at thermoneutral conditions (29 – 31°C) in rested and fasted animals could be conducted to assess the basal metabolic rate. Furthermore, as shown in figure 15 (C) and 19 (C) an adaption phase was visible in the beginning of the metabolic cage trial. Therefore, a habituation phase could be considered by evaluating only days 4 to 8.

The last experiment conducted was fear conditioning, in which associative learning and memory was assessed. Previous observations by Dorninger et al. (2019a) showing reduced freezing responses in contextual fear conditioning and cued fear conditioning in *Gnpat* KO males could be repeated, even though there were differences in the experimental setup. As mentioned above in the social interaction trial Dorninger et al. (2019a) only used male *Gnpat* KO mice and WT littermates. During the training trial in our experiment mice were presented with the CS and US twice, while in Dorninger et al. (2019a) there was only a single CS-US presentation. Also, in the cued fear conditioning trial in our experiment mice were presented with the CS twice, while in Dorninger et al. (2019a) mice were presented with the CS only once.

A variety of neuronal circuits and mechanisms in different parts of the brain were suggested to be involved in fear conditioning. An important brain region in fear learning and memory is the amygdala, more precisely the lateral nucleus of the amygdala, the basal nucleus of the amygdala that both project to the central nucleus of the amygdala. However, not only the amygdala is involved in fear conditioning, but also thalamic regions, primary, secondary and associative auditory cortices and others (Herry and Johansen, 2014). This strengthens the notion that a lack of ether phospholipids not only affects a specific brain region or neuronal circuit but causes a ubiquitous defect.

This study revealed a difference in freezing response during the 2. CS of the cued fear conditioning trial between *Gnpat* KO and *Peds1* KO mice, suggesting a role of non-vinyl ether phospholipids in associative learning and memory. However, this difference between *Gnpat* KO and *Peds1* KO mice was not visible in the 1. CS of the cued fear conditioning trial as well as in the contextual fear conditioning trial. Thus, it is tempting to speculate that the main effect is based on plasmenyl ether phospholipids but also plasmanyl ether phospholipids are of importance. However, a possible influence by confounding factors such as hyperactivity and visual impairments cannot be excluded. A

hearing test should be performed to exclude possible influence due to hearing impairments.

According to our hypothesis the observed behavioral abnormalities in *Gnpat* KO mice are caused by altered membrane properties as consequence of the lack of plasmalogens as well as the absence of vinyl and non-vinyl ether phospholipid mediators. In addition, a disturbed neurotransmitter homeostasis and neurotransmitter release has been observed. Compensatory mechanism that follow such as a rise in phosphatidylethanolamine in the absence of plasmenyl ethanolamine are thought to impact neuronal circuits and mechanisms (Dorninger et al., 2019a, 2015). The observed behavioral abnormalities in *Gnpat* KO mice may also be impacted by phenotypic traits such as visual impairments and hyperactivity. Possible influence due to motor impairment is unlikely as motor impairments in *Gnpat* KO mice can occur after one year in age, whereas our subject mice were between 3-5 months in age. Also, no motor impairments were observed throughout the entire experiment period.
In *Peds1* KO mice the presence of non-vinyl ether phospholipids is thought to lead to different compensatory mechanisms than in *Gnpat* KO mice, subsequently alleviating the observed behavioral abnormalities caused by a complete lack of ether phospholipids. Indeed, our study showed that in social interaction, locomotor activity and cued fear conditioning *Peds1* KO mice seemed to lie between *Gnpat* KO and WT control animals. However, no differences in contextual fear conditioning were seen between *Gnpat* KO and *Peds1* KO. The behavioral observations of *Peds1* KO mice may also be influenced by a suggested attenuated but still hyperactive phenotype. The exact mechanisms behind the alleviation of the behavioral abnormalities in *Peds1* KO mice are still unknown.

In conclusion, this study strengthened previous findings in *Gnpat* KO mice but also gave insight into behavioral changes in *Peds1* KO mice highlighting the importance of non-vinyl ether phospholipids on mouse behavior. In addition, this study allowed insights into the metabolism of *Gnpat* KO and *Peds1* KO mice. In social interaction no significant differences between the groups or within each group were determined. However, a trend was visible with *Peds1* KO seeming to lie between *Gnpat* KO and WT control mice. The metabolic cage showed robust data on significantly increased activity in *Gnpat* KO and *Peds1* KO males as well as metabolic changes in energy expenditure, oxygen consumption, carbon dioxide production and body weight in both genotypes all likely

influenced by the increased activity (except for body weight). Finally, fear conditioning revealed significant reduction in freezing response in both *Gnpat* KO and *Peds1* KO mice in both contextual and cued fear conditioning, suggesting impaired associative learning and memory. However, all results need to be looked at in the context of hyperactivity and visual impairments in *Gnpat* KO mice as well as a suggested attenuated but still hyperactive phenotype in *Peds1* KO mice.

Future studies may focus on identifying the exact role of non-vinyl ether phospholipids in the brain at a molecular level, ideally establishing a causal link with behavioral abnormalities. Even though this might prove to be a challenging task, it would provide a better understanding of the role of ether phospholipids in the brain possibly leading to better treatment options to neurological diseases linked to ether phospholipid deficiency.

5 REFERENCES

Ali, F., Hossain, Md.S., Sejimo, S., Akashi, K., 2019. Plasmalogens Inhibit Endocytosis of Toll-like Receptor 4 to Attenuate the Inflammatory Signal in Microglial Cells. Mol. Neurobiol. 56, 3404–3419. https://doi.org/10.1007/s12035-018-1307-2

Atanasova, E., Arévalo, A.P., Graf, I., Zhang, R., Bockmann, J., Lutz, A.-K., Boeckers, T.M., 2023. Immune activation during pregnancy exacerbates ASD-related alterations in Shank3-deficient mice. Mol. Autism 14, 1. https://doi.org/10.1186/s13229-022-00532-3

Berger, J., Dorninger, F., Forss-Petter, S., Kunze, M., 2016. Peroxisomes in brain development and function. Biochim. Biophys. Acta BBA - Mol. Cell Res. 1863, 934–955. https://doi.org/10.1016/j.bbamcr.2015.12.005

Bi, P., Shan, T., Liu, W., Yue, F., Yang, X., Liang, X.-R., Wang, J., Li, J., Carlesso, N., Liu, X., Kuang, S., 2014. Inhibition of Notch signaling promotes browning of white adipose tissue and ameliorates obesity. Nat. Med. 20, 911–918. https://doi.org/10.1038/nm.3615

Boudina, S., Sena, S., O'Neill, B.T., Tathireddy, P., Young, M.E., Abel, E.D., 2005. Reduced Mitochondrial Oxidative Capacity and Increased Mitochondrial Uncoupling Impair Myocardial Energetics in Obesity. Circulation 112, 2686–2695. https://doi.org/10.1161/CIRCULATIONAHA.105.554360

Braverman, N.E., Moser, A.B., 2012. Functions of plasmalogen lipids in health and disease. Biochim. Biophys. Acta BBA - Mol. Basis Dis. 1822, 1442–1452. https://doi.org/10.1016/j.bbadis.2012.05.008

Braverman, N.E., Raymond, G.V., Rizzo, W.B., Moser, A.B., Wilkinson, M.E., Stone, E.M., Steinberg, S.J., Wangler, M.F., Rush, E.T., Hacia, J.G., Bose, M., 2016. Peroxisome biogenesis disorders in the Zellweger spectrum: An overview of current diagnosis, clinical manifestations, and treatment guidelines. Mol. Genet. Metab. 117, 313–321. https://doi.org/10.1016/j.ymgme.2015.12.009

Braverman, N.E., Steinberg, S.J., Fallatah, W., Duker, A., Bober, M.B., 2001. Rhizomelic Chondrodysplasia Punctata Type 1.

Brodde, A., Teigler, A., Brugger, B., Lehmann, W.D., Wieland, F., Berger, J., Just, W.W., 2012. Impaired neurotransmission in ether lipid-deficient nerve terminals. Hum. Mol. Genet. 21, 2713–2724. https://doi.org/10.1093/hmg/dds097

Chen, Z., Ho, I.-L., Soeung, M., Yen, E.-Y., Liu, J., Yan, L., Rose, J.L., Srinivasan, S., Jiang, S., Edward Chang, Q., Feng, N., Gay, J.P., Wang, Q., Wang, J., Lorenzi, P.L., Veillon, L.J., Wei, B., Weinstein, J.N., Deem, A.K., Gao, S., Genovese, G., Viale, A., Yao, W., Lyssiotis, C.A., Marszalek, J.R., Draetta, G.F., Ying, H., 2023. Ether phospholipids are required for mitochondrial reactive oxygen species

homeostasis. Nat. Commun. 14, 2194. https://doi.org/10.1038/s41467-023-37924-9

Colon-Mesa, I., Sainz, N., Corrales, P., Collantes, M., Kaldis, P., Martinez, J.A., Medina-Gómez, G., Moreno-Aliaga, M.J., Escoté, X., 2023. p27Kip1 Deficiency Impairs Brown Adipose Tissue Function Favouring Fat Accumulation in Mice. Int. J. Mol. Sci. 24, 2664. https://doi.org/10.3390/ijms24032664

Crawley, J.N., 2023. Twenty years of discoveries emerging from mouse models of autism. Neurosci. Biobehav. Rev. 146, 105053. https://doi.org/10.1016/j.neubiorev.2023.105053

da Silva, T.F., Eira, J., Lopes, A.T., Malheiro, A.R., Sousa, V., Luoma, A., Avila, R.L., Wanders, R.J.A., Just, W.W., Kirschner, D.A., Sousa, M.M., Brites, P., 2014. Peripheral nervous system plasmalogens regulate Schwann cell differentiation and myelination. J. Clin. Invest. 124, 2560–2570. https://doi.org/10.1172/JCI72063

De Duve, C., Baudhuin, P., 1966. Peroxisomes (microbodies and related particles). Physiol. Rev. 46, 323–357. https://doi.org/10.1152/physrev.1966.46.2.323

Dean, J.M., Lodhi, I.J., 2018. Structural and functional roles of ether lipids. Protein Cell 9, 196–206. https://doi.org/10.1007/s13238-017-0423-5

Dorninger, F., Brodde, A., Braverman, N.E., Moser, A.B., Just, W.W., Forss-Petter, S., Brügger, B., Berger, J., 2015. Homeostasis of phospholipids — The level of phosphatidylethanolamine tightly adapts to changes in ethanolamine plasmalogens. Biochim. Biophys. Acta BBA - Mol. Cell Biol. Lipids 1851, 117–128. https://doi.org/10.1016/j.bbalip.2014.11.005

Dorninger, F., Forss-Petter, S., Berger, J., 2017. From peroxisomal disorders to common neurodegenerative diseases – the role of ether phospholipids in the nervous system. FEBS Lett. 591, 2761–2788. https://doi.org/10.1002/1873-3468.12788

Dorninger, F., Forss-Petter, S., Wimmer, I., Berger, J., 2020. Plasmalogens, platelet-activating factor and beyond – Ether lipids in signaling and neurodegeneration. Neurobiol. Dis. 145, 105061. https://doi.org/10.1016/j.nbd.2020.105061

Dorninger, F., Gundacker, A., Zeitler, G., Pollak, D.D., Berger, J., 2019a. Ether Lipid Deficiency in Mice Produces a Complex Behavioral Phenotype Mimicking Aspects of Human Psychiatric Disorders. Int. J. Mol. Sci. 20, 3929. https://doi.org/10.3390/ijms20163929

Dorninger, F., König, T., Scholze, P., Berger, M.L., Zeitler, G., Wiesinger, C., Gundacker, A., Pollak, D.D., Huck, S., Just, W.W., Forss-Petter, S., Pifl, C., Berger, J., 2019b. Disturbed neurotransmitter homeostasis in ether lipid deficiency. Hum. Mol. Genet. 28, 2046–2061. https://doi.org/10.1093/hmg/ddz040

Drechsler, R., Chen, S.-W., Dancy, B.C.R., Mehrabkhani, L., Olsen, C.P., 2016. HPLC-Based Mass Spectrometry Characterizes the Phospholipid Alterations in Ether-

Linked Lipid Deficiency Models Following Oxidative Stress. PLOS ONE 11, e0167229. https://doi.org/10.1371/journal.pone.0167229

Duker, A.L., Niiler, T., Eldridge, G., Brereton, N.H., Braverman, N.E., Bober, M.B., 2017. Growth charts for individuals with rhizomelic chondrodysplasia punctata. Am. J. Med. Genet. A. 173, 108–113. https://doi.org/10.1002/ajmg.a.37961

Duker, A.L., Niiler, T., Kinderman, D., Schouten, M., Poll-The, B.T., Braverman, N., Bober, M.B., 2020. Rhizomelic chondrodysplasia punctata morbidity and mortality, an update. Am. J. Med. Genet. A. 182, 579–583. https://doi.org/10.1002/ajmg.a.61413

Engelmann, B., 2004. Plasmalogens: targets for oxidants and major lipophilic antioxidants. Biochem. Soc. Trans. 32, 147–150. https://doi.org/10.1042/bst0320147

Even, P.C., Blais, A., 2016. Increased Cost of Motor Activity and Heat Transfer between Non-Shivering Thermogenesis, Motor Activity, and Thermic Effect of Feeding in Mice Housed at Room Temperature – Implications in Pre-Clinical Studies. Front. Nutr. 3. https://doi.org/10.3389/fnut.2016.00043

Even, P.C., Nadkarni, N.A., 2012. Indirect calorimetry in laboratory mice and rats: principles, practical considerations, interpretation and perspectives. Am. J. Physiol.-Regul. Integr. Comp. Physiol. 303, R459–R476. https://doi.org/10.1152/ajpregu.00137.2012

Farré, J., Mahalingam, S.S., Proietto, M., Subramani, S., 2019. Peroxisome biogenesis, membrane contact sites, and quality control. EMBO Rep. 20. https://doi.org/10.15252/embr.201846864

Fujiki, Y., Okumoto, K., Honsho, M., Abe, Y., 2022. Molecular insights into peroxisome homeostasis and peroxisome biogenesis disorders. Biochim. Biophys. Acta BBA - Mol. Cell Res. 1869, 119330. https://doi.org/10.1016/j.bbamcr.2022.119330

Glaser, P.E., Gross, R.W., 1994. Plasmenylethanolamine Facilitates Rapid Membrane Fusion: A Stopped-Flow Kinetic Investigation Correlating the Propensity of a Major Plasma Membrane Constituent to Adopt an HII Phase with Its Ability to Promote Membrane Fusion. Biochemistry 33, 5805–5812. https://doi.org/10.1021/bi00185a019

Gorgas, K., Teigler, A., Komljenovic, D., Just, W.W., 2006. The ether lipid-deficient mouse: Tracking down plasmalogen functions. Biochim. Biophys. Acta BBA - Mol. Cell Res. 1763, 1511–1526. https://doi.org/10.1016/j.bbamcr.2006.08.038

Hagelkruys, A., Horrer, M., Taubenschmid-Stowers, J., Kavirayani, A., Novatchkova, M., Orthofer, M., Pai, T.-P., Cikes, D., Zhuk, S., Balmaña, M., Esk, C., Koglgruber, R., Moeseneder, P., Lazovic, J., Zopf, L.M., Cronin, S.J.F., Elling, U., Knoblich, J.A., Penninger, J.M., 2022. The HUSH complex controls brain architecture and protocadherin fidelity. Sci. Adv. 8, eabo7247. https://doi.org/10.1126/sciadv.abo7247

Hara-Kuge, S., Fujiki, Y., 2008. The peroxin Pex14p is involved in LC3-dependent degradation of mammalian peroxisomes. Exp. Cell Res. 314, 3531–3541. https://doi.org/10.1016/j.yexcr.2008.09.015

Herry, C., Johansen, J.P., 2014. Encoding of fear learning and memory in distributed neuronal circuits. Nat. Neurosci. 17, 1644–1654. https://doi.org/10.1038/nn.3869

Hofteig, J.H., Noronha, A.B., Druse, M.J., Keresztes-Nagy, C., 1985. Synaptic membrane phospholipids: Effects of maternal ethanol consumption. Exp. Neurol. 87, 165–171. https://doi.org/10.1016/0014-4886(85)90142-6

Honsho, M., Fujiki, Y., 2017. Plasmalogen homeostasis – regulation of plasmalogen biosynthesis and its physiological consequence in mammals. FEBS Lett. 591, 2720–2729. https://doi.org/10.1002/1873-3468.12743

Hossain, Md.S., Abe, Y., Ali, F., Youssef, M., Honsho, M., Fujiki, Y., Katafuchi, T., 2017. Reduction of Ether-Type Glycerophospholipids, Plasmalogens, by NF-κB Signal Leading to Microglial Activation. J. Neurosci. 37, 4074–4092. https://doi.org/10.1523/JNEUROSCI.3941-15.2017

Jiang, L., Hara-Kuge, S., Yamashita, S., Fujiki, Y., 2015. Peroxin Pex14p is the key component for coordinated autophagic degradation of mammalian peroxisomes by direct binding to LC3-II. Genes Cells 20, 36–49. https://doi.org/10.1111/gtc.12198

Jiménez-Rojo, N., Riezman, H., 2019. On the road to unraveling the molecular functions of ether lipids. FEBS Lett. 593, 2378–2389. https://doi.org/10.1002/1873-3468.13465

Jones, J.M., Morrell, J.C., Gould, S.J., 2004. PEX19 is a predominantly cytosolic chaperone and import receptor for class 1 peroxisomal membrane proteins. J. Cell Biol. 164, 57–67. https://doi.org/10.1083/jcb.200304111

Kaidanovich-Beilin, O., Lipina, T., Vukobradovic, I., Roder, J., Woodgett, J.R., 2011. Assessment of Social Interaction Behaviors. J. Vis. Exp. 2473. https://doi.org/10.3791/2473

Kashii, H., Kasai, S., Sato, A., Hagino, Y., Nishito, Y., Kobayashi, T., Hino, O., Mizuguchi, M., Ikeda, K., 2023. Tsc2 mutation rather than Tsc1 mutation dominantly causes a social deficit in a mouse model of tuberous sclerosis complex. Hum. Genomics 17, 4. https://doi.org/10.1186/s40246-023-00450-2

Kemp, S., Berger, J., Aubourg, P., 2012. X-linked adrenoleukodystrophy: Clinical, metabolic, genetic and pathophysiological aspects. Biochim. Biophys. Acta BBA - Mol. Basis Dis. 1822, 1465–1474. https://doi.org/10.1016/j.bbadis.2012.03.012

Koivuniemi, A., 2017. The biophysical properties of plasmalogens originating from their unique molecular architecture. FEBS Lett. 591, 2700–2713. https://doi.org/10.1002/1873-3468.12754

References

Komljenovic, D., Sandhoff, R., Teigler, A., Heid, H., Just, W.W., Gorgas, K., 2009. Disruption of blood-testis barrier dynamics in ether-lipid-deficient mice. Cell Tissue Res. 337, 281–299. https://doi.org/10.1007/s00441-009-0809-7

König, C., Plank, A.-C., Kapp, A., Timotius, I.K., von Hörsten, S., Zimmermann, K., 2020. Thirty Mouse Strain Survey of Voluntary Physical Activity and Energy Expenditure: Influence of Strain, Sex and Day–Night Variation. Front. Neurosci. 14, 531. https://doi.org/10.3389/fnins.2020.00531

Kou, J., Kovacs, G.G., Höftberger, R., Kulik, W., Brodde, A., Forss-Petter, S., Hönigschnabl, S., Gleiss, A., Brügger, B., Wanders, R., Just, W., Budka, H., Jungwirth, S., Fischer, P., Berger, J., 2011. Peroxisomal alterations in Alzheimer's disease. Acta Neuropathol. (Berl.) 122, 271–283. https://doi.org/10.1007/s00401-011-0836-9

Kunze, M., Malkani, N., Maurer-Stroh, S., Wiesinger, C., Schmid, J.A., Berger, J., 2015. Mechanistic Insights into PTS2-mediated Peroxisomal Protein Import. J. Biol. Chem. 290, 4928–4940. https://doi.org/10.1074/jbc.M114.601575

Kurihara, Y., Mitsunari, K., Mukae, N., Shoji, H., Miyakawa, T., Shirane, M., 2023. PDZD8-deficient mice manifest behavioral abnormalities related to emotion, cognition, and adaptation due to dyslipidemia in the brain. Mol. Brain 16, 11. https://doi.org/10.1186/s13041-023-01002-4

Lackner, K., Sailer, S., van Klinken, J.-B., Wever, E., Pras-Raves, M.L., Dane, A.D., Honsho, M., Abe, Y., Keller, M.A., Golderer, G., Werner-Felmayer, G., Fujiki, Y., Vaz, F.M., Werner, E.R., Watschinger, K., 2023. Alterations in ether lipid metabolism and the consequences for the mouse lipidome. Biochim. Biophys. Acta BBA - Mol. Cell Biol. Lipids 1868, 159285. https://doi.org/10.1016/j.bbalip.2023.159285

Lazarow, P.B., Fujiki, Y., 1985. Biogenesis of Peroxisomes. Annu. Rev. Cell Biol. 1, 489–530. https://doi.org/10.1146/annurev.cb.01.110185.002421

Lohner, K., Balgavy, P., Hermetter, A., Paltauf, F., Laggner, P., 1991. Stabilization of non-bilayer structures by the etherlipid ethanolamine plasmalogen. Biochim. Biophys. Acta BBA - Biomembr. 1061, 132–140. https://doi.org/10.1016/0005-2736(91)90277-F

Marvyn, P.M., Bradley, R.M., Mardian, E.B., Marks, K.A., Duncan, R.E., 2016. Data on oxygen consumption rate, respiratory exchange ratio, and movement in C57BL/6J female mice on the third day of consuming a high-fat diet. Data Brief 7, 472–475. https://doi.org/10.1016/j.dib.2016.02.066

Nadler, J.J., Moy, S.S., Dold, G., Simmons, N., Perez, A., Young, N.B., Barbaro, R.P., Piven, J., Magnuson, T.R., Crawley, J.N., 2004. Automated apparatus for quantitation of social approach behaviors in mice. Genes Brain Behav. 3, 303–314. https://doi.org/10.1111/j.1601-183X.2004.00071.x

References

Nagan, N., Zoeller, R.A., 2001. Plasmalogens: biosynthesis and functions. Prog. Lipid Res. 40, 199–229. https://doi.org/10.1016/S0163-7827(01)00003-0

Nakamoto, C., Kawamura, M., Nakatsukasa, E., Natsume, R., Takao, K., Watanabe, M., Abe, M., Takeuchi, T., Sakimura, K., 2020. GluD1 knockout mice with a pure C57BL/6N background show impaired fear memory, social interaction, and enhanced depressive-like behavior. PLOS ONE 15, e0229288. https://doi.org/10.1371/journal.pone.0229288

Oeljeklaus, S., Schummer, A., Mastalski, T., Platta, H.W., Warscheid, B., 2016. Regulation of peroxisome dynamics by phosphorylation. Biochim. Biophys. Acta BBA - Mol. Cell Res. 1863, 1027–1037. https://doi.org/10.1016/j.bbamcr.2015.12.022

Okumoto, K., Tamura, S., Honsho, M., Fujiki, Y., 2020. Peroxisome: Metabolic Functions and Biogenesis, in: Lizard, G. (Ed.), Peroxisome Biology: Experimental Models, Peroxisomal Disorders and Neurological Diseases, Advances in Experimental Medicine and Biology. Springer International Publishing, Cham, pp. 3–17. https://doi.org/10.1007/978-3-030-60204-8_1

Park, H., He, A., Tan, M., Johnson, J.M., Dean, J.M., Pietka, T.A., Chen, Y., Zhang, X., Hsu, F.-F., Razani, B., Funai, K., Lodhi, I.J., 2019. Peroxisome-derived lipids regulate adipose thermogenesis by mediating cold-induced mitochondrial fission. J. Clin. Invest. 129, 694–711. https://doi.org/10.1172/JCI120606

Pignataro, A., Krashia, P., De Introna, M., Nobili, A., Sabetta, A., Stabile, F., La Barbera, L., D'Addario, S.L., Ventura, R., Cecconi, F., D'Amelio, M., Ammassari-Teule, M., 2023. Chemogenetic rectification of the inhibitory tone onto hippocampal neurons reverts autistic-like traits and normalizes local expression of estrogen receptors in the Ambra1+/- mouse model of female autism. Transl. Psychiatry 13, 63. https://doi.org/10.1038/s41398-023-02357-x

Pike, L.J., 2006. Rafts defined: a report on the Keystone symposium on lipid rafts and cell function. J. Lipid Res. 47, 1597–1598. https://doi.org/10.1194/jlr.E600002-JLR200

Pike, L.J., Han, X., Chung, K.-N., Gross, R.W., 2002. Lipid Rafts Are Enriched in Arachidonic Acid and Plasmenylethanolamine and Their Composition Is Independent of Caveolin-1 Expression: A Quantitative Electrospray Ionization/Mass Spectrometric Analysis. Biochemistry 41, 2075–2088. https://doi.org/10.1021/bi0156557

Rapanelli, M., Wang, W., Hurley, E., Feltri, M.L., Pittenger, C., Frick, L.R., Yan, Z., 2023. Cholinergic neurons in the basal forebrain are involved in behavioral abnormalities associated with Cul3 deficiency: Role of prefrontal cortex projections in cognitive deficits. Transl. Psychiatry 13, 22. https://doi.org/10.1038/s41398-023-02306-8

Rhodin, J., 1958. Electron microscopy of the kidney. Am. J. Med. 24, 661–675. https://doi.org/10.1016/0002-9343(58)90373-5

References

Rienecker, K.D.A., Grue, K., Paladini, M.S., Frias, E.S., Frattini, V., Borlongan, M.C., Chou, A., Torres-Espin, A., Krukowski, K., Ferguson, A.R., Rosi, S., 2023. Combined space stressors induce independent behavioral deficits predicted by early peripheral blood monocytes. Sci. Rep. 13, 1749. https://doi.org/10.1038/s41598-023-28508-0

Rodemer, C., Thai, T.-P., Brugger, B., Kaercher, T., Werner, H., Nave, K.-A., Wieland, F., Gorgas, K., Just, W.W., 2003. Inactivation of ether lipid biosynthesis causes male infertility, defects in eye development and optic nerve hypoplasia in mice. Hum. Mol. Genet. 12, 1881–1895. https://doi.org/10.1093/hmg/ddg191

Rubio, J.M., Astudillo, A.M., Casas, J., Balboa, M.A., Balsinde, J., 2018. Regulation of Phagocytosis in Macrophages by Membrane Ethanolamine Plasmalogens. Front. Immunol. 9, 1723. https://doi.org/10.3389/fimmu.2018.01723

Rüdiger, M., Kolleck, I., Putz, G., Wauer, R.R., Stevens, P., Rüstow, B., 1998. Plasmalogens effectively reduce the surface tension of surfactant-like phospholipid mixtures. Am. J. Physiol.-Lung Cell. Mol. Physiol. 274, L143–L148. https://doi.org/10.1152/ajplung.1998.274.1.L143

Salin, K., Villasevil, E.M., Anderson, G.J., Lamarre, S.G., Melanson, C.A., McCarthy, I., Selman, C., Metcalfe, N.B., 2019. Differences in mitochondrial efficiency explain individual variation in growth performance. Proc. R. Soc. B Biol. Sci. 286, 20191466. https://doi.org/10.1098/rspb.2019.1466

Shiwaku, H., Katayama, S., Gao, M., Kondo, K., Nakano, Y., Motokawa, Y., Toyoda, S., Yoshida, F., Hori, H., Kubota, T., Ishikawa, K., Kunugi, H., Ikegaya, Y., Okazawa, H., Takahashi, H., 2023. Analyzing schizophrenia-related phenotypes in mice caused by autoantibodies against NRXN1α in schizophrenia. Brain. Behav. Immun. 111, 32–45. https://doi.org/10.1016/j.bbi.2023.03.028

Sindelar, P.J., Guan, Z., Dallner, G., Ernster, L., 1999. The protective role of plasmalogens in iron-induced lipid peroxidation. Free Radic. Biol. Med. 26, 318–324. https://doi.org/10.1016/S0891-5849(98)00221-4

Spiers, J.G., Chen, H.-J.C., Steyn, F.J., Lavidis, N.A., Woodruff, T.M., Lee, J.D., 2017. Noninvasive assessment of altered activity following restraint in mice using an automated physiological monitoring system. Stress 20, 76–84. https://doi.org/10.1080/10253890.2016.1276898

Stoll, C., Dott, B., Roth, M.-P., Alembik, Y., 2008. Birth prevalence rates of skeletal dysplasias. Clin. Genet. 35, 88–92. https://doi.org/10.1111/j.1399-0004.1989.tb02912.x

Takamori, S., Holt, M., Stenius, K., Lemke, E.A., Grønborg, M., Riedel, D., Urlaub, H., Schenck, S., Brügger, B., Ringler, P., Müller, S.A., Rammner, B., Gräter, F., Hub, J.S., De Groot, B.L., Mieskes, G., Moriyama, Y., Klingauf, J., Grubmüller, H., Heuser, J., Wieland, F., Jahn, R., 2006. Molecular Anatomy of a Trafficking Organelle. Cell 127, 831–846. https://doi.org/10.1016/j.cell.2006.10.030

References

Teigler, A., Komljenovic, D., Draguhn, A., Gorgas, K., Just, W.W., 2009. Defects in myelination, paranode organization and Purkinje cell innervation in the ether lipid-deficient mouse cerebellum. Hum. Mol. Genet. 18, 1897–1908. https://doi.org/10.1093/hmg/ddp110

Vamecq, J., Cherkaoui-Malki, M., Andreoletti, P., Latruffe, N., 2014. The human peroxisome in health and disease: The story of an oddity becoming a vital organelle. Biochimie 98, 4–15. https://doi.org/10.1016/j.biochi.2013.09.019

Wanders, R.J.A., Baes, M., Ribeiro, D., Ferdinandusse, S., Waterham, H.R., 2023. The physiological functions of human peroxisomes. Physiol. Rev. 103, 957–1024. https://doi.org/10.1152/physrev.00051.2021

Wanders, R.J.A., Waterham, H.R., 2006. Biochemistry of Mammalian Peroxisomes Revisited. Annu. Rev. Biochem. 75, 295–332. https://doi.org/10.1146/annurev.biochem.74.082803.133329

Wang, B., Tontonoz, P., 2019. Phospholipid Remodeling in Physiology and Disease. Annu. Rev. Physiol. 81, 165–188. https://doi.org/10.1146/annurev-physiol-020518-114444

Wang, J., Cao, Y., Hou, W., Bi, D., Yin, F., Gao, Y., Huang, D., Li, Y., Cao, Z., Yan, Y., Zhao, J., Kong, D., Lv, X., Huang, L., Zhong, H., Wu, C., Chen, Q., Yang, R., Wei, Q., Qin, H., 2023. Fecal microbiota transplantation improves VPA-induced ASD mice by modulating the serotonergic and glutamatergic synapse signaling pathways. Transl. Psychiatry 13, 17. https://doi.org/10.1038/s41398-023-02307-7

Waterham, H.R., Ferdinandusse, S., Wanders, R.J.A., 2016. Human disorders of peroxisome metabolism and biogenesis. Biochim. Biophys. Acta BBA - Mol. Cell Res. 1863, 922–933. https://doi.org/10.1016/j.bbamcr.2015.11.015

Weir, J.B. de V., 1949. New methods for calculating metabolic rate with special reference to protein metabolism. J. Physiol. 109, 1–9. https://doi.org/10.1113/jphysiol.1949.sp004363

Werner, E.R., Keller, M.A., Sailer, S., Lackner, K., Koch, J., Hermann, M., Coassin, S., Golderer, G., Werner-Felmayer, G., Zoeller, R.A., Hulo, N., Berger, J., Watschinger, K., 2020. The *TMEM189* gene encodes plasmanylethanolamine desaturase which introduces the characteristic vinyl ether double bond into plasmalogens. Proc. Natl. Acad. Sci. 117, 7792–7798. https://doi.org/10.1073/pnas.1917461117

Yang, M., Silverman, J.L., Crawley, J.N., 2011. Automated Three-Chambered Social Approach Task for Mice. Curr. Protoc. Neurosci. 56. https://doi.org/10.1002/0471142301.ns0826s56

Youssef, M., Ibrahim, A., Akashi, K., Hossain, M.S., 2019. PUFA-Plasmalogens Attenuate the LPS-Induced Nitric Oxide Production by Inhibiting the NF-kB, p38 MAPK and JNK Pathways in Microglial Cells. Neuroscience 397, 18–30. https://doi.org/10.1016/j.neuroscience.2018.11.030

Yu, T.W., Chahrour, M.H., Coulter, M.E., Jiralerspong, S., Okamura-Ikeda, K., Ataman, B., Schmitz-Abe, K., Harmin, D.A., Adli, M., Malik, A.N., D'Gama, A.M., Lim, E.T., Sanders, S.J., Mochida, G.H., Partlow, J.N., Sunu, C.M., Felie, J.M., Rodriguez, J., Nasir, R.H., Ware, J., Joseph, R.M., Hill, R.S., Kwan, B.Y., Al-Saffar, M., Mukaddes, N.M., Hashmi, A., Balkhy, S., Gascon, G.G., Hisama, F.M., LeClair, E., Poduri, A., Oner, O., Al-Saad, S., Al-Awadi, S.A., Bastaki, L., Ben-Omran, T., Teebi, A.S., Al-Gazali, L., Eapen, V., Stevens, C.R., Rappaport, L., Gabriel, S.B., Markianos, K., State, M.W., Greenberg, M.E., Taniguchi, H., Braverman, N.E., Morrow, E.M., Walsh, C.A., 2013. Using Whole-Exome Sequencing to Identify Inherited Causes of Autism. Neuron 77, 259–273. https://doi.org/10.1016/j.neuron.2012.11.002